Synthesis and Characterization of Magnesium-Manganese-Based Oxide on Nickel Foam for Electrochemical CO_2 Reduction to Formate

ADITTYA CHOWDHURY JOY

SUPERVISOR
Foysal Kabir Tareq
Souman Rudra
Tore Sandnes Vehus
Prasanjit Das

University of Agder, 2024
Faculty of Engineering and Science
Department of Engineering Sciences

UiA University of Agder

Master

Copyright Declaration

I hereby declare that I am the sole author of the thesis titled "**Synthesis and Characterization of Magnesium-Manganese Based Oxide on Nickel Foam for electrochemical CO_2 reduction to formate"**. Along with this, submitted a softcopy is true copy of my final hardcopy thesis including any required final revisions, as accepted by the board of examination.

I hereby release my copyright to **Chittagong University of Engineering and Technology (CUET)** for uploading the electronic version of the same to the **'Digital Repository (Institutional Repository)'** of **CUET** after one year from the day of submission. Apart from this, the existing or to be approved **Open Education Resources (OER)** policies and procedures of **Chittagong University of Engineering and Technology (CUET)** shall be applicable to this research work.

I also acknowledge my sincere delivering of copyright to Chittagong University of Engineering and Technology (CUET) to reproduce this thesis by reprography or by other means, in total or by part at the necessity of individuals for the purpose of scholarly research.

…….

Signature of the Author

Abstract

The increasing levels of atmospheric CO_2 from industrial activities necessitate effective technologies to mitigate climate change. Electrochemical CO_2 reduction offers a promising route to convert CO_2 into valuable products like formate, but challenges such as high overpotential, low selectivity, and catalyst instability hinder its efficiency. Conventional catalysts, while effective, often suffer from low performance or high costs, driving the search for alternative materials. This research explores magnesium-manganese oxide-based catalysts on nickel foam, leveraging their synergistic effects, unique structural properties, and cost-effectiveness to enhance Electrochemical CO_2 reduction efficiency. The catalysts were directly grown on nickel foam via immersion in a precursor solution followed by calcination at 600°C. Structural and compositional analysis through X-ray diffraction (XRD), scanning electron microscopy (SEM), and energy-dispersive X-ray spectroscopy (EDS) confirmed the formation of crystalline phases, including Ni_6MnO_8, NiO, and $NiMnO_3$, with magnesium likely incorporated into the manganese oxide lattice. SEM revealed coral reef-like morphology, while elemental analysis indicated a uniform distribution of magnesium (1.1%) and manganese (22.1%) within the porous nickel foam. The optimized catalyst, Mg1.1-Mn22.1-Ox/NiF, exhibited superior electrocatalytic performance, achieving a high current density of -63.24 mA cm^{-2} at -0.85 V vs. RHE and a low onset potential of 0.07 V, indicating improved charge transfer capabilities. These findings highlight the structural and compositional advantages of magnesium integration, significantly enhancing catalytic activity and stability. This work provides valuable insights into the design of advanced electrocatalysts for efficient CO_2 reduction, paving the way for further optimization and exploration of magnesium-manganese-based oxides systems.

বিমূর্ত

শিল্প কার্যক্রম থেকে নির্গত বায়ুমণ্ডলীয় কার্বন ডাই অক্সাইডের এর ক্রমবর্ধমান মাত্রা জলবায়ু পরিবর্তন মোকাবিলায় কার্যকর প্রযুক্তির প্রয়োজনীয়তা সৃষ্টি করেছে। ইলেক্ট্রোকেমিক্যাল কার্বন ডাই অক্সাইড রিডাকশন কার্বন ডাই অক্সাইডকে ফরমেটের মতো মূল্যবান পণ্যতে রূপান্তরের একটি সম্ভাবনাময় পদ্ধতি হলেও, উচ্চ ওভারপোটেনশিয়াল, নিম্ন সিলেক্টিভিটি এবং ক্যাটালিস্টের স্থায়িত্বজনিত সীমাবদ্ধতা এর কার্যকারিতা ব্যাহত করে। প্রচলিত ক্যাটালিস্ট কার্যকর হলেও, কম কর্মক্ষমতা বা উচ্চ ব্যয়ের কারণে বিকল্প উপাদানের সন্ধান অপরিহার্য হয়ে উঠেছে। এই গবেষণায় নিকেল ফোমে ম্যাগনেশিয়াম-ম্যাঙ্গানিজ অক্সাইড ভিত্তিক ক্যাটালিস্টের উন্নয়ন এবং তার ইলেক্ট্রোকেমিক্যাল কার্বন ডাই অক্সাইড রিডাকশন দক্ষতা বৃদ্ধির সম্ভাবনা অনুসন্ধান করা হয়েছে। ক্যাটালিস্টটি একটি প্রিকার্সার দ্রবণে নিমজ্জিত করে ৬০০°C তাপমাত্রায় ক্যালসিনেশন প্রক্রিয়ার মাধ্যমে সরাসরি নিকেল ফোমে বৃদ্ধি করা হয়। কাঠামোগত ও উপাদানগত বিশ্লেষণের জন্য এক্স রে ডিফ্র্যাকশন (এক্স আর ডি), স্ক্যানিং ইলেক্ট্রন মাইক্রোস্কপি (এস ই এম), এবং এনার্জি ডিস্পারসিভ এক্স রে স্প্যাকট্রস্কপি (ই ডি এস) ব্যবহার করা হয়েছে। ফলাফল অনুসারে, Ni_6MnO_8, NiO, এবং $NiMnO_3$ সহ বিভিন্ন স্ফটিক পর্যায় গঠিত হয়েছে, যেখানে ম্যাগনেশিয়াম সম্ভবত ম্যাঙ্গানিজ অক্সাইডের ল্যাটিসে অন্তর্ভুক্ত হয়েছে। এস ই এম বিশ্লেষণে প্রবাল প্রাচীর সদৃশ কাঠামো দেখা গেছে, এবং উপাদান বিশ্লেষণে ম্যাগনেশিয়াম (১.১%) ও ম্যাঙ্গানিজ (২২.১%) এর অভিন্ন বণ্টন নিশ্চিত হয়েছে। উন্নত ক্যাটালিস্ট, Mg1.1-Mn22.1-Ox/NiF, উল্লেখযোগ্য ইলেক্ট্রোক্যাটালিটিক কর্মক্ষমতা প্রদর্শন করেছে, যেখানে -০.৮৫ V vs. RHE এ -৬৩.২৪ mA cm^{-2} উচ্চ বর্তমান ঘনত্ব এবং ০.০৭ V নিম্ন অনসেট পোটেনশিয়াল অর্জিত হয়েছে, যা উন্নত চার্জ স্থানান্তর ক্ষমতা নির্দেশ করে। এই গবেষণার ফলাফল ম্যাগনেশিয়ামের সংযোজন দ্বারা কাঠামোগত ও উপাদানগত সুবিধাগুলি উন্মোচিত করেছে, যা ক্যাটালিটিক কার্যকারিতা ও স্থায়িত্বকে উল্লেখযোগ্যভাবে উন্নত করেছে। এই কাজটি উন্নত ইলেক্ট্রোক্যাটালিস্ট ডিজাইনের ক্ষেত্রে মূল্যবান অন্তর্দৃষ্টি প্রদান করে এবং ভবিষ্যতে ম্যাগনেশিয়াম-ম্যাঙ্গানিজ ভিত্তিক অক্সাইড সিস্টেমের অপ্টিমাইজেশন ও অনুসন্ধানের সম্ভাবনা উন্মোচন করে।

Preface

This thesis work was successfully accomplished under the project “Collaborative Action for improving Educational capacities in Renewable Energy to mitigate climate crisis (CARE)” between Chittagong University of Engineering and Technology (CUET), Bangladesh and University of Agder (UIA), Norway (Collaboration Agreement No. NORPART-2021/10355).

I would like to convey my heartfelt gratitude to my supervisors, Foysal Kabir Tareq, Souman Rudra and Tore Sandnes Vehus, from the Department of Engineering Sciences, University of Agder for their excellent guidance, supervision and valuable advice throughout the project. I am also grateful to Prof. Prasanjit Das and Dr. Abu Shadat Muhammad Sayem, from the Department of Mechanical Engineering, Chittagong University of Engineering and Technology, for his motivation and mentorship during my thesis work.

I want to express my gratitude to Md Iftekher Hossain, from the University of Agder who assisted me in completing the M.Sc. thesis.

I want to express my deepest gratitude to my father, my mother, and my sisters for their unwavering support and encouragement during my educational pursuit. Devoid of their assistance, I would have been unable to attain this stage.

I want to express my heartfelt appreciation to everyone for their assistance with technical matters and their moral encouragement and helpful advice in the thesis work.

Adittya Chowdhury Joy
University of Agder, Norway
Grimstad, December 2024

Individual/group Mandatory Declaration

The individual student or group of students is responsible for the use of legal tools, guidelines for using these and rules on source usage. The statement will make the students aware of their responsibilities and the consequences of cheating. Missing statement does not release students from their responsibility.

1.	I/We hereby declare that my/our report is my/our own work and that I/We have not used any other sources or have received any other help than mentioned in the thesis.	☒
2.	I/we further declare that this thesis: - has not been used for another exam at another department/university/university college in Norway or abroad; - does not refer to the work of others without it being stated; - does not refer to own previous work without it being stated; - have all the references given in the literature list; - is not a copy, duplicate or copy of another's work or manuscript.	☒
3.	I/we am/are aware that violation of the above is regarded as cheating and may result in cancellation of exams and exclusion from universities and colleges in Norway, see Universitets- og høgskoleloven §§4-7 og 4-8 og Forskrift om eksamen §§ 31.	☒
4.	I/we am/are aware that all submitted theses may be checked for plagiarism.	☒
5.	I/we am/are aware that the University of Agder will deal with all cases where there is suspicion of cheating according to the university's guidelines for dealing with cases of cheating.	☒
6.	I/we have incorporated the rules and guidelines in the use of sources and references on the library's web pages.	☒

Publishing Agreement

Authorization for electronic publishing of the thesis.

Author(s) have copyrights of the thesis. This means, among other things, the exclusive right to make the work available to the general public (Åndsverkloven. §2).

All theses that fulfill the criteria will be registered and published in Brage Aura and on UiA's web pages with author's approval.

Theses that are not public or are confidential will not be published.

I hereby give the University of Agder a free right to

make the task available for electronic publishing: ☒JA ☐NEI

Is the thesis confidential? ☐JA ☒NEI

(confidential agreement must be completed and signed by the Head of the Department)

- If yes:

Can the thesis be published when the confidentiality period is over? ☐JA ☐NEI

Is the task except for public disclosure? ☐JA ☒NEI

(contains confidential information. see Offl. §13/Fvl. §13)

Table of Contents

List of Figures

Chapter 1

Introduction

1.1 Background

Advocating for net zero emissions is essential for stabilizing global temperatures and addressing climate change. Net-zero emission manifests when reduced greenhouse gases (GHGs) from the atmosphere outweigh the GHGs produced by human activities. Net zero signifies that the total emissions introduced into the atmosphere are equivalent to the total emissions extracted, leading to no net augmentation of atmospheric greenhouse gases, particularly focusing on carbon dioxide (CO_2) [1]. To fulfill the Paris Agreement's objective of constraining the rise in global warming to 1.5°C, worldwide CO_2 emissions must become net zero by the mid-21st century, with other greenhouse gases afterward. Even after reaching net zero, the climate system may continue to evolve, necessitating ongoing monitoring and adjustments to emissions strategies. This holistic strategy is essential to address climate change properly. The notion of net-zero emissions extends beyond specific nations or regions. This necessitates significant modifications in energy generation, utilization, and human activities [2].

The phenomenal economic advancement and population growth worldwide have resulted in a significant need for energy, emerging as a global concern. Conventional fossil fuels have been extensively utilized and overexploited, leading to numerous issues such as environmental degradation, global warming, and shortages of fossil fuels. Due to elevated energy demands, the combustion of fossil fuels such as coal, petroleum, and natural gas has been the primary source of greenhouse gases (GHGs) [3]. As shown in Figure 1, CO_2, a significant greenhouse gas, contributes to global warming, climate change, rise in sea level which will significantly jeopardize the survival of both animals and people on Earth [4]. Moreover, new research demonstrates that elevated atmospheric CO_2 concentrations might adversely impact plant growth, leading to diminished food yields and nutritional quality [5]. The rise in atmospheric CO_2 concentrations, chiefly attributable to fossil fuel consumption, deforestation, and industrial activities, has resulted in substantial environmental alterations, including extreme weather phenomena and rising sea levels. Consequently, it is imperative to diminish CO_2 emissions while concurrently transforming into favorable items for the welfare of the environment [6].

Two fundamental approaches show promise in reducing CO_2 levels: (i) CO_2 collection and geological storage, and (ii) the conversion of CO_2 gas into valuable fuels and goods. The conversion and utilization of CO_2 as a fuel source appear appealing and promising in the current context of elevated energy demands [7]. The growing need to provide sustainable energy solutions has spurred research into carbon capture and utilization (CCU) technologies, emphasizing the electrochemical reduction of CO_2. To mitigate the extra atmospheric CO_2 burden, carbon capture and utilization (CCU) is a viable technical approach that reduces greenhouse gas emissions and ozone depletion. One option to address this is the electrochemical conversion of CO_2 into useful compounds using renewable energy. This process is

essential for transforming CO_2 into many useful compounds and fuels. Formic acid, methanol, and ethylene function as energy transporters and feedstocks in chemical synthesis while providing economic advantages for CO_2 usage [8].

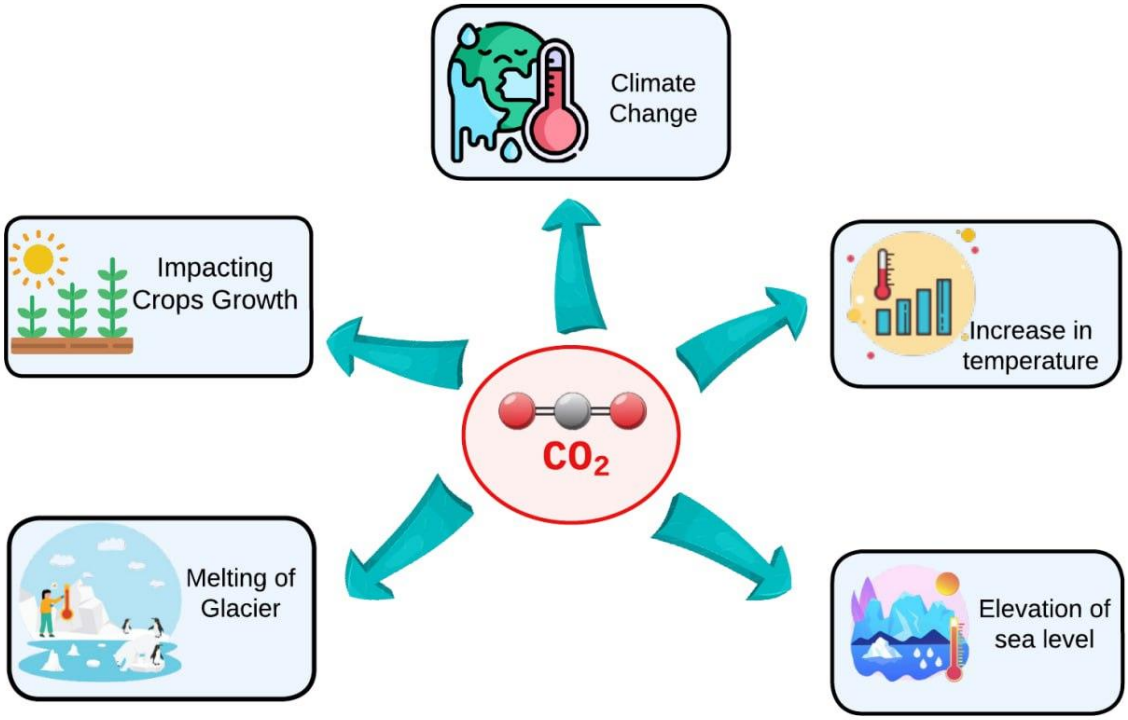

Figure 1. Detrimental effects of excessive emission of CO_2

On the other hand, the conversion and subsequent utilization of CO_2 necessitates various energy sources to surmount kinetic inertia and the thermodynamic energy barrier. Methods such as Fischer-Tropsch synthesis [9], CO_2 mineralization [10], and catalytic hydrogenation [11] are among the industrially implemented techniques. As the procedure of these conventional approaches necessitates catalytic materials and elevated temperatures due to the exceptional stability of CO_2, their limits cannot be overstated. However, currently, strategies utilizing innovative alternatives such as biochemical [12], photochemical [13], plasma-based technology [14], and electrochemical methods [15] are being extensively developed.

The electrochemical CO_2 reduction reaction technique has attracted noteworthy recognition due to its multiple advantages as follows – (1) the process is controlled by the voltage applied to electrodes, (2) electrolyte solution can be recycled and so chemical consumption is minimized, (3) new sources of electricity can be used [16]. Electrochemical CO_2 reduction has markedly advanced in recent years. The industrial usage of this technology predominantly depends on the activity, selectivity, and robustness of various proton and electron chemical processes. In this case, the techno-economic feasibility of CO_2 electrochemical reduction is heavily contingent upon the end products, which serve as critical productivity benchmarks propelling this technological approach toward profitability. This is evident due to the swift advancement of renewable energy infrastructure [17].

The electrochemical conversion of carbon dioxide (CO_2) gas into value-added products in aqueous solution is a crucial technique for utilizing CO_2 as a carbon-neutral energy source and alleviating the

energy crisis. The electrochemical CO_2 reduction reaction (CO2RR) can produce numerous compounds, including carbon monoxide (CO), methane (CH_4), formic acid (HCOOH), and other hydrocarbons, contingent upon the materials and reaction potential employed [18].

Formic acid (HCOOH), a byproduct of CO2RR, possesses significant market potential due to its high energy density for use as a hydrogen carrier in fuel cells [19]. Nevertheless, the hydrogen evolution reaction (HER) transpires concurrently as a competing process; hence, HER must be mitigated to achieve higher catalytic activity in converting CO_2 to HCOOH.

Metal oxide materials possess potential applications in electrochemistry, including catalysis and environmental remediation. They are categorized into single metal oxides, spinel oxides, chalcogenide oxides, metal oxides with unique structures, metal layered hydroxides, and oxide-containing hybrids based on their structural variety and composition [20]. Transition metal oxide (TMO) is an easily obtainable material characterized by its high surface area, rapid reaction rate, magnetic separability, low cost, straightforward surface functionalization, minimal biological toxicity, and high environmental stability and adsorption capacity [21]. Noble metal-based electrocatalysts, including Pd [22], Ag [23], Au [24], and their alloys, have demonstrated activity for CO_2 reduction reactions in aqueous solutions at low overpotentials. It is more beneficial to create effective and selective electrocatalysts for CO_2 reduction reactions utilizing inexpensive and abundantly available metals.

The transition metal manganese (Mn) ranks third in natural abundance among transition elements, following iron and titanium [25]. Mn-based oxides have been extensively documented as electrocatalytic materials, particularly as CO_2 reduction reaction (CO2RR) catalysts, owing to their affordability, elevated electrochemical activity, commendable stability, diverse crystal structures, tunable morphological sizes, and variable manganese ion valence states [26]. To confirm the statement, Mn-oxide-based OER catalysts have been reported as key factors affecting electrochemical performance [27].

In addition, Magnesium oxide-based materials possess numerous advantages, including high theoretical capture efficiency, cost-effectiveness, accessibility, environmental friendliness, non-corrosiveness, and broad applicability [28]. Consequently, MgO-based adsorbents have been identified as a viable choice for CO_2 collection at moderate temperatures. MgO is a widely accessible alkaline metal oxide and is characterized by a broad band gap [29].

Meanwhile, Current collectors utilized in different electrochemical systems comprise metal foams (e.g., Ni, Al, Fe), metal sheets (Pt, Ti, Cu), carbon cloth, non-stick tape, and stainless steel. Among them, Nickel foam has garnered interest due to their effective electrode configuration, resulting from their interconnected three-dimensional (3D) architecture, as well as their ability to establish a robust connection between the active material and the external circuit [30]. Furthermore, NF exhibits advantageous characteristics like exceptional mechanical strength, notable electrical and thermal conductivity, minimal ionic diffusion resistance, commendable corrosion resistance, and enhanced areal loading of active materials [31].

1.2 Aims and objectives

The aim of this study is to design highly active manganese-based oxide on nickel foam for electrochemical CO_2 reduction to formate. The aim will be achieved through the following objectives.

1. Develop and optimize a magnesium manganese-based oxide catalyst on nickel foam and perform structural, morphological, and compositional characterization to ensure effective material design.
2. Assess the catalytic activity of the synthesized material for electrochemical CO_2 reduction, focusing on onset potential, overpotential and current density.
3. Analyze the products of electrochemical CO_2 reduction using Fourier Transform Infrared Spectroscopy.

1.3 Research questions

1. How can magnesium-manganese oxide catalysts on nickel foam be synthesized and characterized to optimize their structural, morphological, and compositional properties for?
2. How do unique structural, morphological, and compositional properties of materials influence the electrochemical CO_2 reduction?
3. What are the key electrochemical performance metrics, such as onset potential, overpotential, and current density, for magnesium-manganese oxide catalysts in CO_2 reduction, and how can these be optimized?
4. What products are formed during the electrochemical reduction of CO_2 using magnesium-manganese oxide catalysts, and how can their composition and selectivity be accurately analyzed?

1.4 Thesis Outline

This thesis consists of five chapters.

Chapter 1: Presents an introduction and background information on the selected problem and the objectives of this research followed by research questions.

Chapter 2: Presents a comprehensive classification of CO_2 reduction and possible pathways and related terms.

Chapter 3: Outlines the methodology, preparation and characterization procedures used for the experiment.

Chapter 4: The chapter concludes by examining the physical and electrochemical testing.

Chapter 5: Provides a concise summary of our findings and proposes more research opportunities.

Chapter 2

Theoretical Background

2.1 Fundamental Information of CO_2

In the early 17th century, Jan B. van Helmont identified carbon monoxide as a distinct gas following his examination of its production during combustion and fermentation. This significant discovery established the basis for additional scientific investigation into the characteristics and functions of CO_2 in numerous natural systems and industrial uses [32]. CO_2 is a colorless and odorless gas. The molecule is linear, including a double bond between the carbon and oxygen atoms. CO_2 is the most oxidized form of carbon with a formal oxidation state of +4. CO_2, an outcome of the burning of hydrocarbon compounds, possesses a molecular structure where carbon is in its maximum oxidation state, with a standard Gibbs free energy ΔG_f of −394.38 kJ/mol. Thus, it is thermally stable and chemically inert. Furthermore, carbon atoms in the CO_2 molecule possess vacant p-orbitals, which exhibit a limited capacity for electron acceptance. However, under specific conditions, the inclusion of an electron into the antibonding orbital of CO_2 results in the transformation of the straight CO_2 molecule into the bent $CO_2^{\bullet -}$ anion. This leads to a decrease in the C-O bond order from 2 to 1.5 in the CO_2 molecule, therefore facilitating the activation of inert carbon dioxide molecules [33]. The conversion of CO_2 into a more energetic product necessitates the transfer of electrons to carbon, therefore decreasing its oxidation state. The sequence of steps that transform CO_2 into a more reduced product can be referred to as CO_2 reduction. CO_2 provides a supply of carbon for the photosynthesis of plants and crops. These reactions are sometimes termed CO_2 hydrogenation, meaning thermally driven processes that involve reactions with hydrogen (H_2) or CO_2 fixation in natural photosynthesis catalysis [34]. For the formation and the following combustion of CO_2 reduction/hydrogenation products to constitute a closed cycle, the primary source of electrons and protons for CO_2 reduction must be water (H_2O), as the burning of a hydrogenated carbon product generates H_2O. The general formula for CO_2 reduction, hydrogenation, and fixation is as follows:

$$xCO_2 + yH_2O \rightarrow \text{Product} + zO_2 \quad (1)$$

2.2 Fundamentals of electrochemical CO_2 reduction reaction

Electrochemical techniques are the most advantageous, necessitating reduced energy and offering superior control over the resultant products. In comparison to other solutions, the electrochemical route is the most promising alternative for CO_2 reduction, as it does not necessitate high temperatures or pressures for efficient reduction, integrates water as a proton source, and enables greater product selectivity than other reduction methods. CO_2 can be trapped and transformed into valuable products, thereby diminishing its concentration. This procedure transforms CO_2 into valuable chemicals such as hydrocarbons and organic compounds through an electrochemical device including three electrodes: (1) Cathode: the site of CO_2 reduction, (2) Anode: the site of oxidation processes, (3) Reference Electrode: assess the reaction potential. The technique is scalable for industrial applications in

machines known as electrolysers, which utilize energy from renewable sources such as sun and wind. In a CO_2 electrolyser at ambient temperature, CO_2 is reduced to various products at the cathode by a CO_2 reduction reaction as in Eq. (2). (CO2RR), while H_2O is oxidized at the anode according to the oxygen evolution reaction (OER) as in Eq. (3).

$$xCO_2 + nH^+ + ne^- \rightarrow \text{Product} + H_20 \quad (2)$$

$$2H_20 \rightarrow O_2 + 4H^+ + 4e^-; E^o = 1.23\ V \quad (3)$$

The four key steps in electrochemical CO_2 reaction are as follows: (1) Chemical adsorption of CO_2 molecules adhere to the catalyst's active sites, (2) The C=O bond in CO_2 is cleaved via electron transport to generate $CO_2^{\bullet -}$ radical for CO_2 activation, (iii) new bonds (C-C or C-H) are established to synthesize hydrocarbons, and (iv) Desorption of final products into the electrolyte from active site [35]. The electrolyte employed is a CO_2 saturated aqueous solution. The oxygen evolution reaction (OER) transpires in the anode compartment, whereas the hydrogen evolution reaction (HER) and the CO_2 reduction process take place in the cathode compartment. The inclusion of water in the electrolyte complicates CO_2 reduction due to the hydrogen evolution reaction (HER), where hydrogen predominates and competes with the CO_2 reduction mechanism [36].

2.3 Classification of electrochemical CO_2 reduction

Electrochemical CO_2 reduction reaction classification generally entails different factors regarding the product, electrolyser, substrate, electrolyte and catalyst (Figure 2).

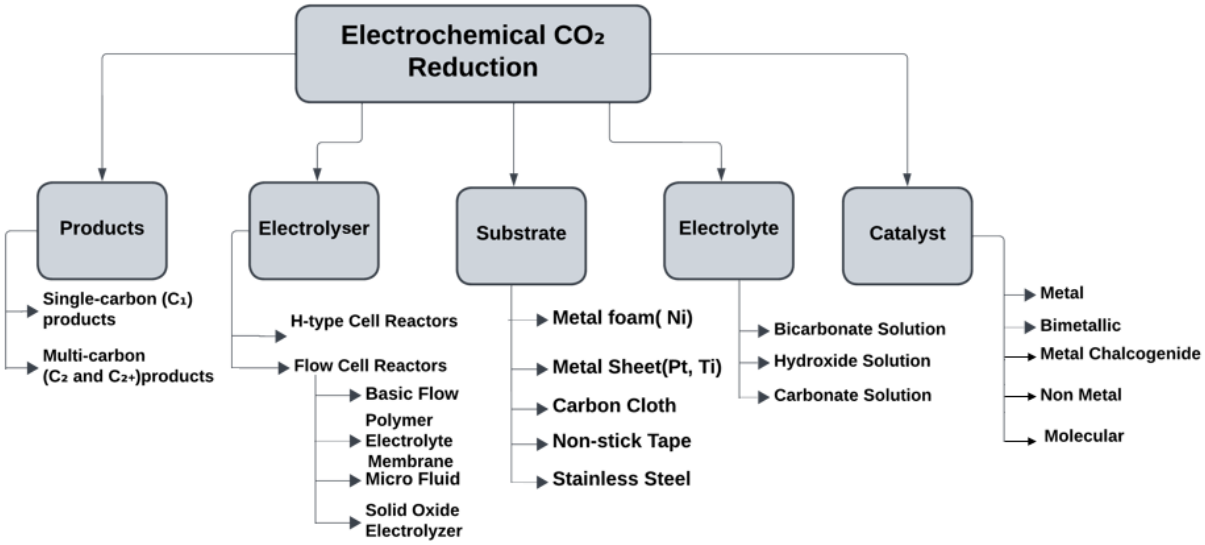

Figure 2. Classification of electrochemical CO_2 reduction from different perspectives [37]

2.4 Products of electrochemical CO_2 reduction reaction

The reaction has several steps involving the transfer of numerous protons and electrons, with electricity supplied to facilitate the electrolytic reaction that generates fuels or chemical commodities. In addition to primary products (carbon monoxide, formic acid, methanol, methane, ethylene, ethanol, and propanol), up to 16 distinct CO_2-derived chemicals, including glyoxal, ethylene glycol, acetaldehyde, and propionaldehyde, have been documented in the literature. Nonetheless, these supplementary products are predominantly documented in trace quantities [37]. Two-electron transfer products, including carbon monoxide (CO) and formate ($HCOO^-$, or formic acid in acidic conditions, HCOOH), are efficiently produced on various catalysts with great selectivity. Various electron-transfer products, such as methanol, methane, ethanol (C_2H_5OH), ethylene (C_2H_4), and propanol (C_3H_8O), have thus far been generated with diminished selectivity.
Figure 3 outlines the primary product coming from the electrochemical CO_2 reaction based on the number of transferred electrons and their respective current production method in the industrial sector [38].

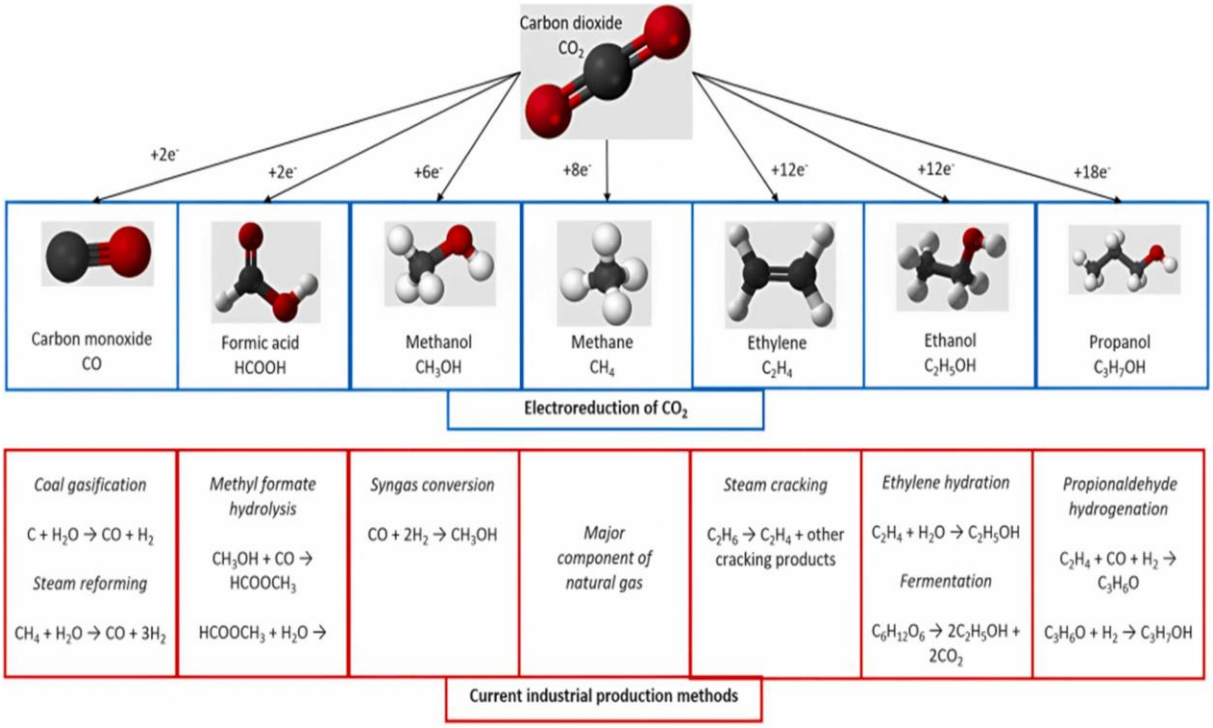

Figure 3. Primary products from electrochemical CO_2 reduction and respective current production method

For a chemical reaction to begin, the Gibbs free energy (or Helmholtz free energy at constant volume) of the products must be less than that of the reactants. The system's free energy must be reduced. Several options exist to accomplish this: through temperature, reactant/product concentrations, applied electrochemical potential, and so on. Table 1 shows a sequence of products that can be obtained as described through successive proton and electron transfers. These compounds can be categorized based on the protonation of the CO_2 molecule and the quantity of carbon.

Table 1: CO_2 reduction reactions to various products and their conventional thermodynamic potentials [39], [40].

Reaction	E°/V vs. SHE	
$CO_2 + 2H^+ + 2e^- \rightarrow HCOOH$	-0.66	(4)
$CO_2 + 2H^+ + 2e^- \rightarrow CO + H_2O$	-0.52	(5)
$CO_2 + 4H^+ + 4e^- \rightarrow CH_2O + H_2O$	-0.49	(6)
$CO_2 + 6H^+ + 6e^- \rightarrow CH_3OH + H_2O$	-0.40	(7)
$CO_2 + 8H^+ + 8e^- \rightarrow CH_4 + 2H_2O$	-0.25	(8)

2.5 Physical characterization

Physical characterization entails an in-depth analysis of the physical properties and structures of materials. This procedure is essential in multiple domains. This thesis encompasses the following aspects of physical characterization:

2.5.1 X-ray diffraction

X-ray diffraction (XRD) is a robust and largely utilized analytical method for analyzing the atomic arrangement within a crystalline substance. XRD is extensively used to determine crystal structures, phases, preferred crystal orientations (texture), and other structural parameters such as average grain size, crystallinity, strain, and crystal defects [41]. Powder X-ray diffraction is commonly used in this regard.

2.5.2 Scanning electron microscope

Scanning Electron Microscope (SEM) deploys a concentrated stream of high-energy electrons to examine the surface of a specimen. The interaction of the electron beam with the sample produces many signals, such as secondary electrons, backscattered electrons, and X-rays, which are utilized to create pictures and assess the sample's composition and surface topography. SEM offers precise images of surface morphology and can assess the chemical composition of the material [42].

2.5.3 Energy dispersive spectroscopy

Energy Dispersive Spectroscopy (EDS) is a widespread analytical method for ascertaining the elemental composition of materials. It is frequently combined with Scanning Electron Microscopes (SEM) and Transmission Electron Microscopes (TEM) to deliver holistic chemical analysis. It is being used to identify and quantify components in a sample by detecting distinctive X-rays generated when the sample is subjected to high-energy electron bombardment [43].

2.6 Electrochemical characterization

Electrochemical characterization is a prerequisite for investigating and improving the performance of various materials and applications. Here, all electrochemical characterizations were conducted utilizing a two-compartment electrochemical cell shown in Figure 3, whereby the working and counter electrodes each were separated by a Nafion 117 membrane. The Ag/AgCl (saturated in 3M KCl)

electrode and platinum wire were demonstrated as the reference and counter electrode respectively. All potentials and current densities present in this study were versus reversible hydrogen electrode (RHE) and geometric surface area (1 cm^2) of the working electrode immersed in the electrolyte. Measured potentials (E(vs Ag/AgCl)) were converted to the reversible hydrogen electrode (RHE) by using the Nernst equation [44].

$$E\ (vs\ RHE) = E\ (vs\ Ag/Agcl) + 0.059pH + 0.197\ [44] \quad (9)$$

The specific electrochemical characterization methods used include the following.

2.6.1 Linear sweep voltammetry

Linear Sweep Voltammetry (LSV) is an electrochemical method used to investigate redox processes by providing a linearly changing voltage to a working electrode and measuring its corresponding current. This method is typical owing to its simplicity, cost-efficiency, and capacity to provide complete understanding into electrochemical processes. LSV necessitates simple but cost-effective instrumentation, rendering it suitable for many applications [45].

2.6.2 Cyclic voltammetry

Cyclic Voltammetry (CV) is a widely used technique in electrochemical research. This technique regulates the electrode potential to perform many scans at varying rates and captures the current-potential curve. Analyze the curve's form to ascertain the events occurring at the electrode. This method was employed to evaluate the redox characteristics of the electrode [46].

2.6.3 Chrono amperometry

Chronoamperometry (CA) is an electrochemical technique used to measure the current response of an electrochemical system to a step change in potential. In CA, the potential of the working electrode is stepped from an initial value to a final value, and the resulting current is recorded over time [47].

2.7 Performance criteria

In electrochemical CO_2 reduction reaction, various metrics have been implemented to evaluate process performance, including current density and onset potential.

2.7.1. Current density

Current density (J) quantifies the electric current (I) per unit area of cross-section (A) in an electrochemical cell, generally represented as Am^{-2} and used as $mAcm^{-2}$ in this work. The current density in CO2RR indicates the reaction rate. Comprehending current density is imperative for enhancing the efficiency and expense of electrochemical electrolyzers. The border region of the catalyst interface demonstrates the maximum current density owing to enhanced conditions for conductivity and mass transfer. A greater current density typically indicates a rapid reaction [48].

2.7.2 Onset potential

The onset potential is the minimum (for anodic reactions) or maximum (for cathodic reactions) potential at which an electrochemical reaction initiates at a specified electrode under established conditions i.e. a lower onset potential (more positive or less negative) signifies that the reaction necessitates reduced energy for initiation, suggesting a more effective catalyst [49]. It is generally calculated in volts (V) in relation to reversible hydrogen electrode. It is essential for evaluating the efficacy of various electrocatalysts.

2.7.3 Overpotential

Overpotential is the additional potential necessary beyond the thermodynamic equilibrium potential to facilitate an electrochemical reaction at a specified rate. It signifies the energy loss inside the system and serves as an indicator of the reaction's inefficiency. Assessing and mitigating overpotential is crucial for enhancing the efficiency of electrochemical systems [50].

2.8 Electrolysers in CO_2 reduction

Recent scientific developments have resulted in the creation of several electrolyser designs, such as H-Cell reactors and flow reactors. Innovations in key components, such as membrane electrode assemblies and gas diffusion electrodes, enhance the stability, current density, faradaic efficiency (FE), and overall efficiency of these electrolysers, while tackling critical issues like solubility and mass transport [51] .

2.8.1 H-type cell

H-Cell reactors have become commercially accessible laboratory-scale reactors that are highly versatile in accommodating various geometries and electrodes. The configuration consists of two chambers containing electrolyte. The cathodic compartment comprises a reference electrode and a working electrode, whereas the counter electrode is in the anodic compartment [52]. The compartments are linked by an ion exchange membrane, forming an H-form that limits the crossover of reduced products and inhibits their further oxidation. The configuration of an H-Cell reactor is depicted in Figure 4 [53]. An H-Cell electrolyser provides an effective method for rapidly evaluating many catalysts.

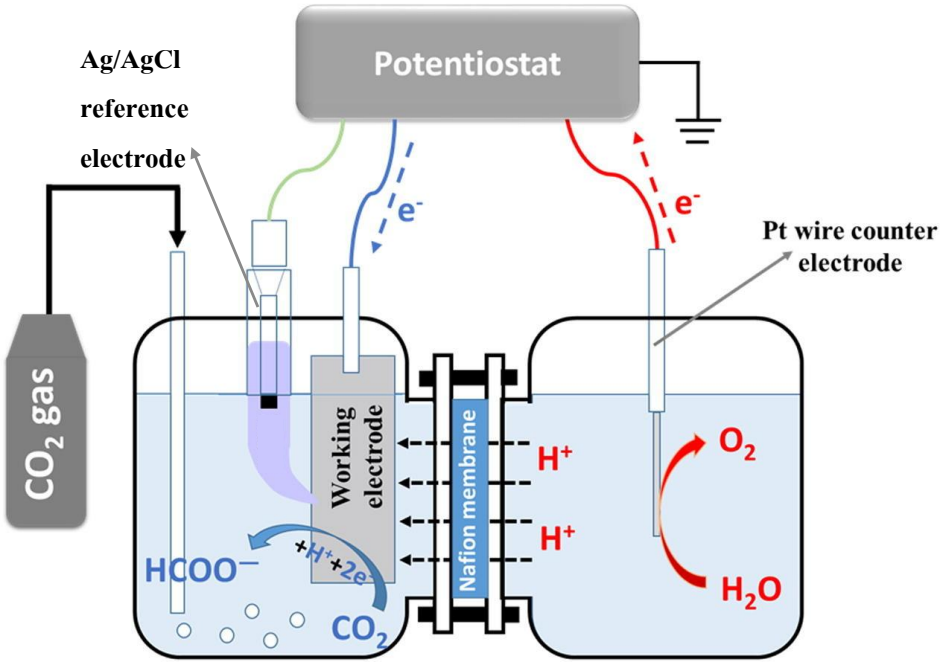

Figure 4. Schematic representation of H-type electrochemical cell [53]

2.9 Role of electrolyte in CO_2 reduction

Electrolytes utilized in electrochemical cells can be categorized into two primary types: aqueous and non-aqueous electrolytes. Among aqueous electrolytes, sodium bicarbonate ($NaHCO_3$) and potassium bicarbonate ($KHCO_3$), with concentrations ranging from 0.1 M to 0.5 M, are the commonly used electrolytes. Bicarbonate electrolytes are comparatively economical, manageable, environmentally benign, and capable of sustaining the pH level within the cell [54].

2.10 Role of substrate in CO_2 reduction

Research on electrochemical systems prioritizes the development of electrode materials that provide cost-effectiveness, stability, and dependable outcomes suitable for commercial scalability. Nonetheless, the functionality of these systems is dependent upon further various elements including electrode production, electrolytes, system design, system durability, and substrate or current collector). Current collectors implemented in distinct electrochemical systems incorporate metal

foams (e.g., Ni, Al, Fe), metal sheets (Pt, Ti, Cu), carbon cloth, non-stick tape, and stainless steel. Nickel foam (NiF) has garnered significant interest as a preferred substrate for numerous electrochemical systems in the selection of current collectors [55]. This emerging trend is ascribed to its notable interconnected three-dimensional architecture, which provides benefits like low weight, high porosity, substantial mechanical strength, chemical stability, and potential electrical and thermal conductivity. These characteristics are advantageous for optimizing contact areas among the current collector, active materials, and charged species, hence minimizing charge transport paths, which is essential for enhancing electrochemical performance.

2.11 Role of catalyst in CO_2 reduction

Recent studies have extensively explored catalysts such as silver (Ag), gold (Au), nickel (Ni), monoatomic catalysts, and bimetallic catalysts. Among them, Bimetallic catalysts outperform monometallic ones due to Electronic effects (modifying electron density), Geometrical effects (enhanced active site arrangement), Synergistic effects, such as Improved formation of catalytic intermediates or Increased surface contact, leading to enhanced activity, selectivity, and stability. By incorporating metal oxides, the electrochemical system can reduce the overpotential and improves current density during CO_2RR [56]. Core–shell nanostructures (e.g., Au nanocrystal@MnO_2 nanosheets) may enhance electrocatalytic performance where the Au core increases electrical conductivity, facilitating rapid electron transfer and the MnO_2 shell can activate CO_2 molecules and stabilizes intermediates like $CO_2^{\cdot-}$. For this specific reason, future studies should focus on understanding the electronic properties of metal oxides and developing advanced nanostructures for better catalytic activity, selectivity, and durability.

Chapter 3

Methodology

3.1 Flowchart of the experiment

This flowchart in Figure 5 outlines a systematic research process for investigating electrochemical CO_2 reduction, starting with a literature review to identify critical pathways, performance criteria, catalysts, electrolyzers, electrolytes, and substrates. It proceeds with the sample preparation and synthesis of materials, followed by material characterization using techniques such as XRD (to analyze crystallinity), SEM (to examine surface morphology), and EDS (to determine elemental composition). Electrochemical testing evaluates the material's performance, and comparative data analysis benchmarks the results against existing studies. Product analysis, using tools like FTIR, identifies and quantifies the chemical products formed. This comprehensive approach ensures a thorough evaluation and optimization of materials and processes, concluding with actionable findings.

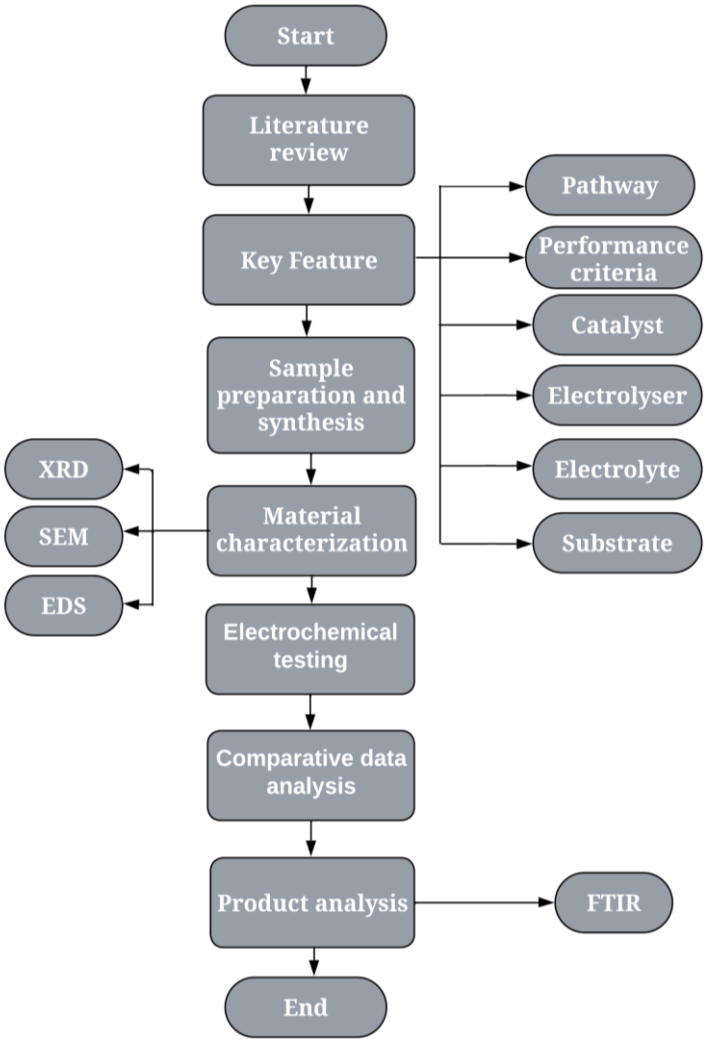

Figure 5. Flow diagram of methodology

3.2 Chemicals and materials

All chemicals used in this study were of reagent grade and utilized without further purification. Manganese(II) nitrate tetrahydrate ($Mn(NO_3)_2{\cdot}4H_2O$, CAS number: 20694-39-7, molecular weight: 251.01 g/mol, ≥97.0% purity, Sigma-Aldrich, Darmstadt, Germany), magnesium chloride hexahydrate ($MgCl_2{\cdot}6H_2O$, CAS number: 7791-18-6, molecular weight: 203.30 g/mol, 99% purity, VWR International, Belgium), Eethylene glycol ($HO\text{-}CH_2\text{-}CH_2\text{-}OH$, CAS Number: 107-21-1, molecular weight: 62.07 g/mol, 99.8% purity, Sigma Aldrich, USA), formic acid 98% (HCOOH, CAS Number: 64-18-6, molecular weight: 46.03 g/mol, ≥88% purity, VWR International, France), sodium bicarbonate ($NaHCO_3$, CAS Number: 144-55-8, molecular weight: 84.01 g/mol, 99.9% purity, Merck, Germany) were procured and used as received. Nickel foam (NiF) with a thickness of 1.6 mm, a bulk density of 0.45 gcm^{-3} and a porosity of 95% was sourced from Sunshinelation, China. Nafion perfluorinated membrane N117 (thickness: 0.005 inches) was purchased from Sigma-Aldrich. High-purity CO_2 (99.99%) and N_2 (99.99%) were procured from a commercial source. All aqueous solutions used in this work were prepared using de-ionized water to ensure the highest level of purity and consistency.

3.3 Preparation and synthesis of catalysts

A 30 mL aqueous solution of $Mn(NO_3)_2{\cdot}4H_2O$ separately and $MgCl_2{\cdot}6H_2O$ and $Mn(NO_3)_2{\cdot}4H_2O$ together was prepared considering a molar concentration ratio of Mg and Mn to be 0.5:1 and 1:1. 3 mL Ethylene Glycol and 2 mL Formic Acid 98% were added and then a piece of NiF (3 cm x 2 cm) was completely immersed into the solution and heated for 45 minutes at 80°C. Finally, after this process, NiF was taken out from the solution and calcined at 600℃ for 4 hours in the muffle furnace at a constant heating rate of 5℃/min. The obtained catalysts were then removed from the muffle furnace and used for further work i.e. characterization and electrochemical testing. As a reference, Mga-Mnb-Ox was named after the different amounts of weight percentage gained from EDS analysis where 'a' is the weight percentage of Mg and 'b' is the weight percentage of Mn in different samples. For that, as we have 4 samples including bare NiF, they are named NiF (only bare NiF), Mn-Ox/NiF (having molar concentration ratio of Mg and Mn to be 0:1), Mg1.1-Mn22.1-Ox/NiF (having molar concentration ratio of Mg and Mn to be 0.5:1) and Mg2-Mn23.7-O_x/NiF (having molar concentration ratio of Mg and Mn to be 1:1) respectively. A schematic illustration of the synthesis process is shown in Figure 6.

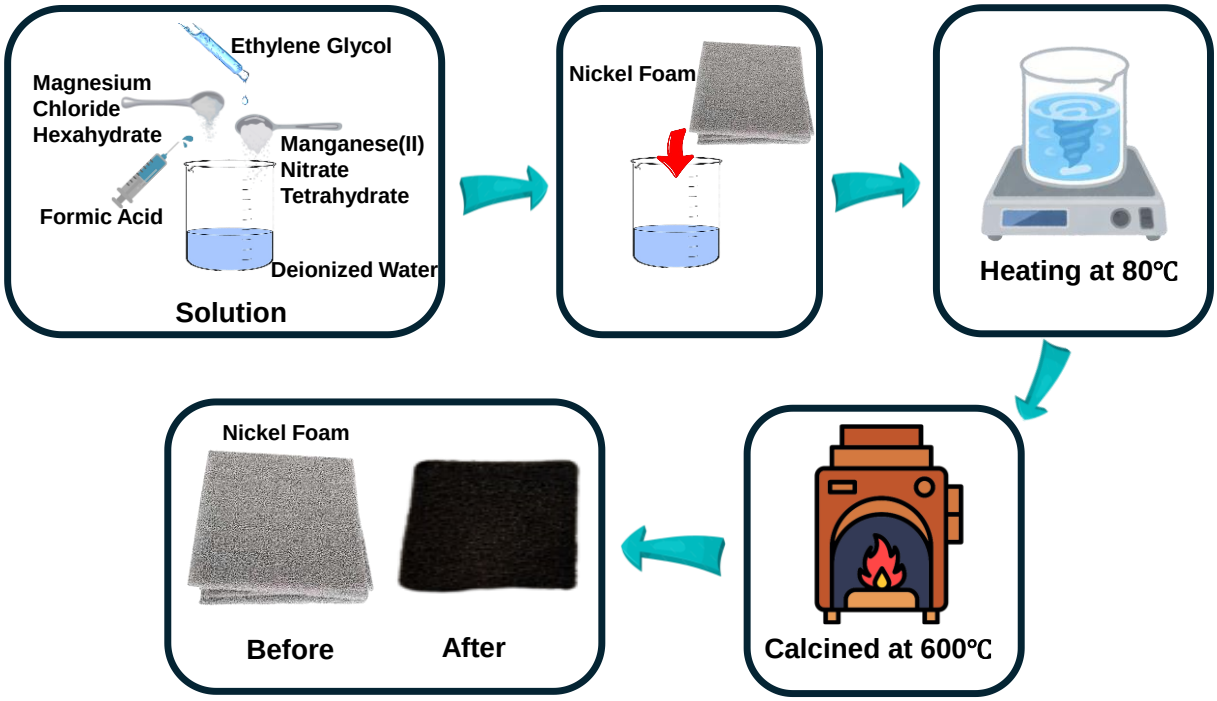

Figure 6. Schematic illustration of the synthesis process of the experiment

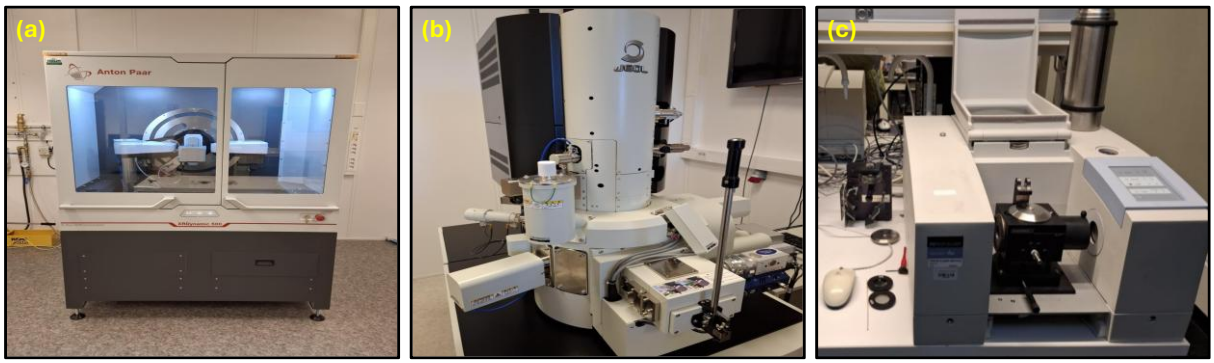

Figure 7. Used instruments in the experiment (a) X-ray Diffractometer (b) Scanning electron microscope (c) Fourier transform infrared spectroscopy

3.4 Characterization techniques

The as-prepared electrocatalysts were characterized to observe the crystalline phase and morphology and elemental composition study by different physicochemical techniques like X-ray diffraction (XRD), field emission scanning electron microscope (FE-SEM) equipped with energy-dispersive X-ray spectroscopy (EDS) detector.

3.4.1 Crystalline phase study

To investigate the crystalline structures, an X-ray diffractometer (XRD) device in Figure 7(a), (XRDynamic 500, Anton Paar) was utilized with Cu Kα radiation at a wavelength of 0.15406 nm. Scans were performed with a diffraction angle range from 10° to 80° with a step size of 0.01° and a scan time of 30 sec per step along with the voltage (40 keV) and current (49 mA).

3.4.2 Morphology and elemental composition Study

The surface morphologies of the materials were characterized using a field emission scanning electron microscope (SEM) model JEOL JSM-7200F (Figure 7(b)), which operated at 15 kV and was equipped with a back-scattered electron (BSE) detector. Additionally, the composition of the materials was analyzed using the same SEM, which was also equipped with an energy dispersive X-ray spectroscopy (EDS) detector.

3.5 Electrochemical characterization

The electrochemical performance of the prepared electrodes was performed using a three-electrode configuration on an electrochemical workstation named IVIUMSTAT (Figure 8(a)). In this process, the NiF coated with Mn and Mg oxide was used as a working electrode, platinum wire served as a counter electrode (Figure 8(c)), and an Ag/AgCl (3M KCl) was used as a reference electrode. All electrochemical studies were accomplished in an aqueous solution containing 0.5 M NaHCO3 (pH 8.35) as a supporting electrolyte. The saturated electrolyte was accompanied by using CO_2 and Ar gases during the electrochemical performance separately. The cathode and the anode compartments were separated by an ion exchange membrane (Nafion Membrane N117). Subsequently, linear sweep voltammetry (LSV), chronoamperometry (CA), and cyclic voltammetry (CV) tests were carried out. Before the electrochemical CO_2 reduction, the Pt electrode was washed with di-ionized water. Firstly, CO_2 gas was bubbled in the cathode compartment for half an hour while stirring the catholyte. All experiments were performed at room temperature under ambient pressure. In the cell, the anode and cathode were separated by the Nafion membrane N117. The electrochemical CO_2 reduction was carried out in a laboratory-made customized H-type cell as shown in Figure 4. All conditions used for the electrochemical reduction of CO_2 are shown in Table 2.

Figure 8. Used instruments in the experiment (a) electrochemical workstation (b) portable single gas detector (c) platinum wire as counter electrode

Table 2: Experimental conditions used for electrochemical CO_2 reduction

Parameter	**Details**
Electrochemical cell for reduction	H-type glass cell
Potentiostat	Ivium
Proton exchange membrane	Nafion membrane N117
Operating Temperature	At room temperature
Potential	−0.85 V (vs RHE)
Working electrode	Electrocatalyst on Ni foam
Counter electrode	Pt wire
Reference electrode	Ag/AgCl (3M KCl)
Catholyte	0.5 M $NaHCO_3$
Anolyte	0.5 M $NaHCO_3$
Carbon dioxide	99.99% Purity
Liquid product analysis	FTIR

3.6 Product analysis study

The thick liquid samples from the experiments were analyzed using a PerkinElmer Spectrum One FT-IR spectrometer equipped with a Harrick single reflectance attenuated total internal reflectance (ATR) accessory and liquid nitrogen cooled MCT detector (Figure 7(c)). Each of the samples was positioned on the ATR crystal using a blunt glass rod. The sample was applied on the crystal, and the sample's spectrum was recorded in the range of 4000–600 cm^{-1}. The background was measured with the ATR crystal before the application of the sample. A total of 32 scans at a resolution of 4 cm^{-1} were made on each sample. The infrared spectra in absorbance format were used in the comparison of the functional groups in the samples.

Chapter 4

Results and Discussion

4.1 Material characterizations

4.1.1 Crystalline phase analysis

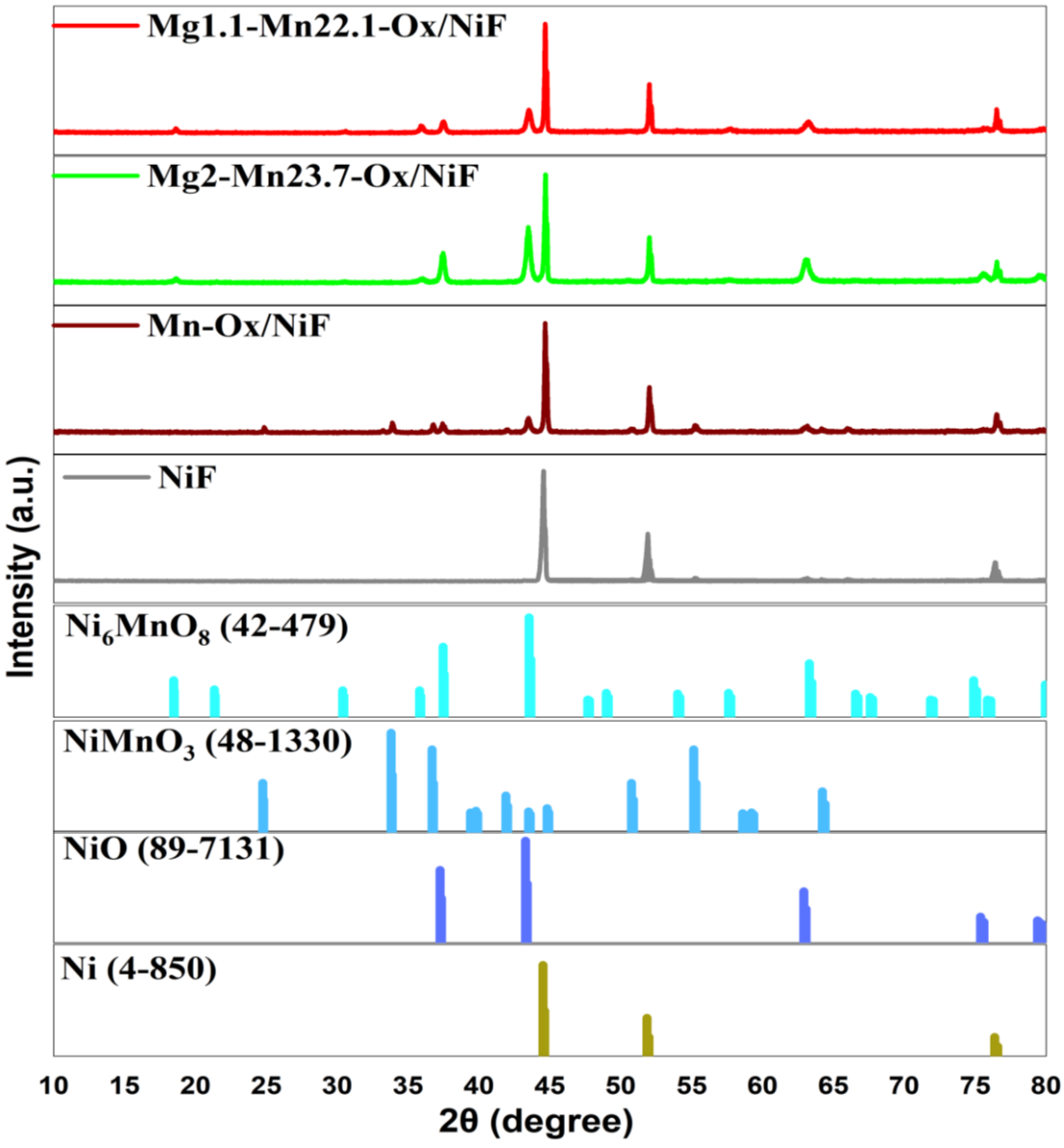

Figure 9. XRD pattern of Mg1.1-Mn22.1-Ox/NiF, Mg2-Mn23.7-Ox/NiF, Mn-Ox/NiF and NiF including crystallographic reference data for Ni_6MnO_8, $NiMnO_3$, NiO and Ni phases

X-ray diffraction (XRD) patterns were used to characterize the crystal phase structure of the NiF, as-prepared Mn-Ox/NiF, Mg2-Mn23.7-Ox/NiF, Mg1.1-Mn22.1-Ox/NiF samples shown in Figure 9. For the NiF, used as a substrate, three obvious characteristic sharp peaks at 2θ = 44.5°, 51.9°, and 76.4° were observed, corresponding to the (111), (200), and (220) planes, respectively, of metallic Ni (JCPDS 850) [57] and the peaks remain as well for other samples too.

In the XRD pattern of Mn-Ox/NiF, except for the diffraction peaks of NiF, it showed the XRD pattern of NiO (JCPDS No. 89-7131) and $NiMnO_3$(JCPDS No. 48-1330) where five peaks at 2θ = 37.4°, 43.5°, 63.1°, 75.5° and 79.80° were noticed which were indexed to (111), (200), (220), (311) and (222) planes of NiO respectively [58] and at 2θ = 24.8°, 33.8°, 36.8°, 42°, 50.7°, 55.2°, 64.1° and 66° were attributed to (110), (121), (-110), (120), (220), (231), (130) and (-211) planes of NiMnO3 respectively [59].

The XRD pattern of Mg2-Mn23.7-Ox/NiF and Mg1.1-Mn22.1-Ox/NiF peaked at the same angle. This means no new peak formation has been observed due to a change in molar concentration or weight percentage. At 2θ = 18.6°, 30.6°, 36° and 57.8° which are introduced here after the first 2 samples indicate the corresponding (111), (220), (311), and (511) planes of Ni_6MnO_8 respectively. The XRD patterns of the samples: Mn-Ox/NiF, Mg2-Mn23.7-Ox/NiF, and Mg1.1-Mn22.1-Ox/NiF are partially overlapped with NiO, $NiMnO_3$, Ni_6MnO_8. The reason is between 500°C and 700°C, there exists a coexistence of NiO, $NiMnO_3$, and Ni_6MnO_8, accompanied by an increase in peak intensity with rising calcination temperature [60]. In our case, the calcination temperature is 600°C.

No significant diffraction peaks of magnesium-related compounds were detected for Mg2-Mn23.7-Ox/NiF and Mg1.1-Mn22.1-Ox/NiF samples indicating that magnesium is adsorbed in the Mn-Ox without forming any crystal [61], [62]. The lack of Mg-related compounds in the XRD patterns, despite the incorporation of Mg into the samples, may be ascribed to the position of Mg in the Mn oxide lattice. The observation is that Mg might take place in the lattice of Mn oxide.

4.1.2 Surface morphology analysis

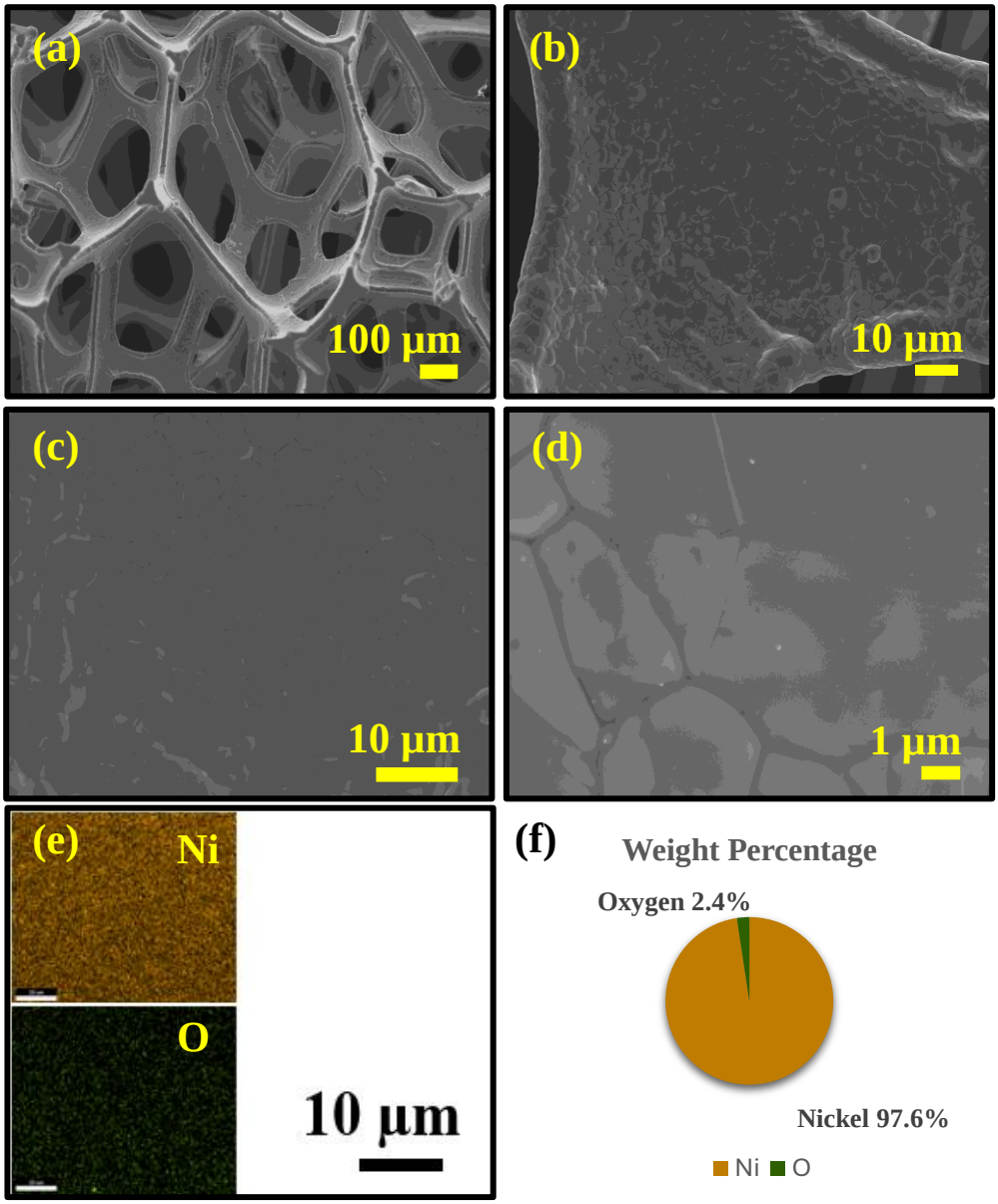

Figure 10. SEM images (a-d) at different magnifications, (e) EDS mapping and (f) weight percentage of NiF

The surface morphology of the NiF and the synthesized catalysts was analyzed using field-emission scanning electron microscopy (FE-SEM) equipped with a back-scattered electron (BSE) detector and energy-dispersive X-ray spectroscopy (EDS). The SEM images of the raw nickel foam at various magnifications are displayed in Figures 10(a-d). The nickel template features a crosslinked, cellular structure with numerous pores that have smooth surfaces. This structure provides ample surface sites for electronic transport. Additionally, the unique porous architecture maximizes the contact area between the collector and the active material, while simultaneously reducing the diffusion and migration distances of electrolyte ions, thereby enhancing electrochemical performance. However, as the sample is exposed to air or moisture during handling, the nickel foam is prone to surface oxidation. This phenomenon is confirmed by the EDS analysis shown in Figures 10(e-f), where the percentages of nickel and oxygen were found to be 97.6% and 2.4%, respectively.

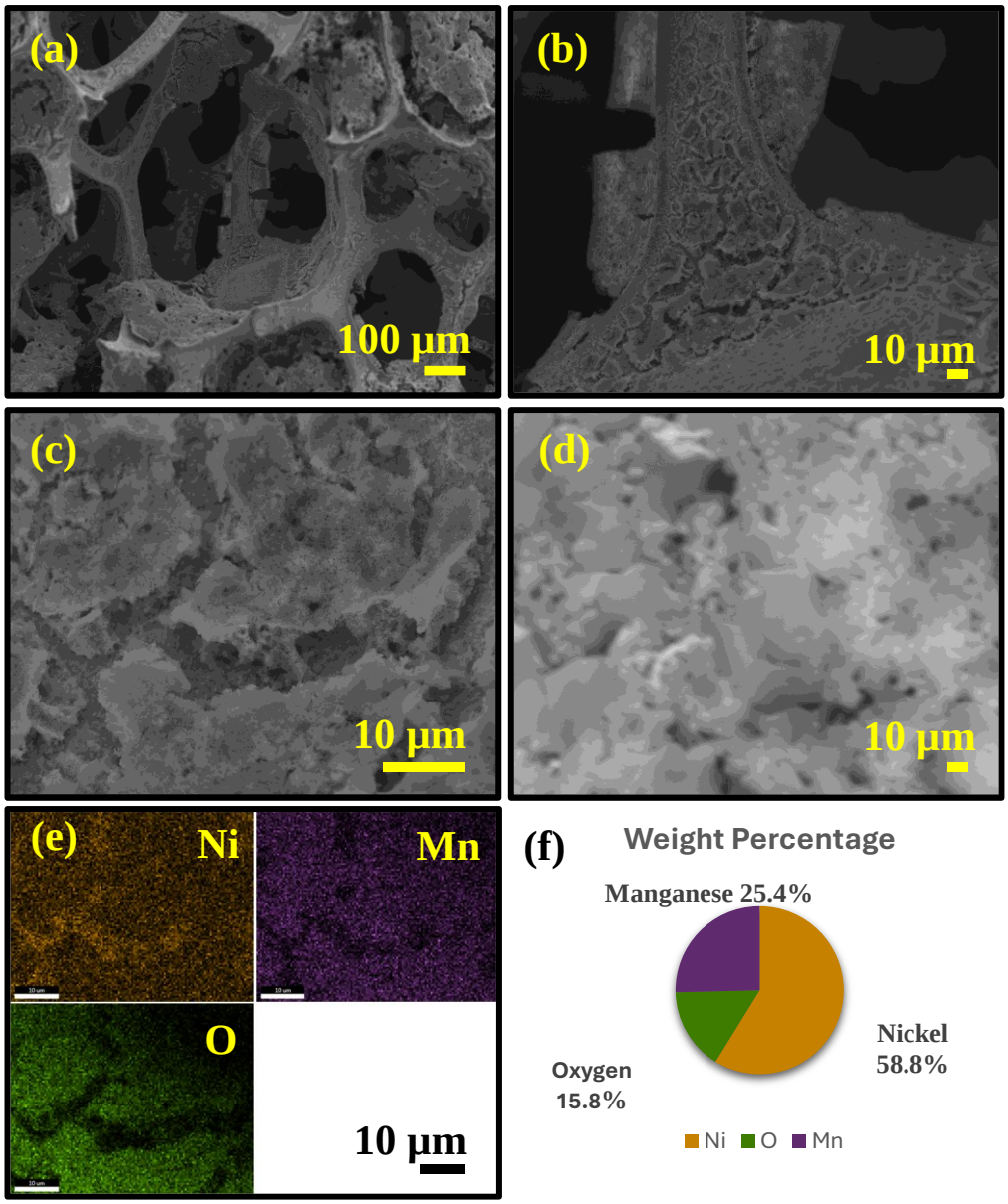

Figure 11. SEM images (a-d) different magnifications, (e) EDS mapping and (f) weight percentage of Mn-Ox/NiF

The SEM images of Mn-Ox on the nickel foam substrate, shown in Figure 11(a-d), revealed a significant amount of oxide formation with a higher density that grew uniformly on the nickel foam. The surface displayed greater roughness compared to that of pure nickel foam, indicating effective adsorption of manganese derived from the oxide [64]. Thermal-induced cracking is evident on the Mn-Ox surface, as indicated by EDS mapping. This mapping in Figure 11(e-f) showed that while 25.4% manganese was present, the cracked areas contained 58.8% nickel, confirming the formation of Mn oxide on nickel foam. The percentage of oxygen about 15.8% depicted the formation of oxides.

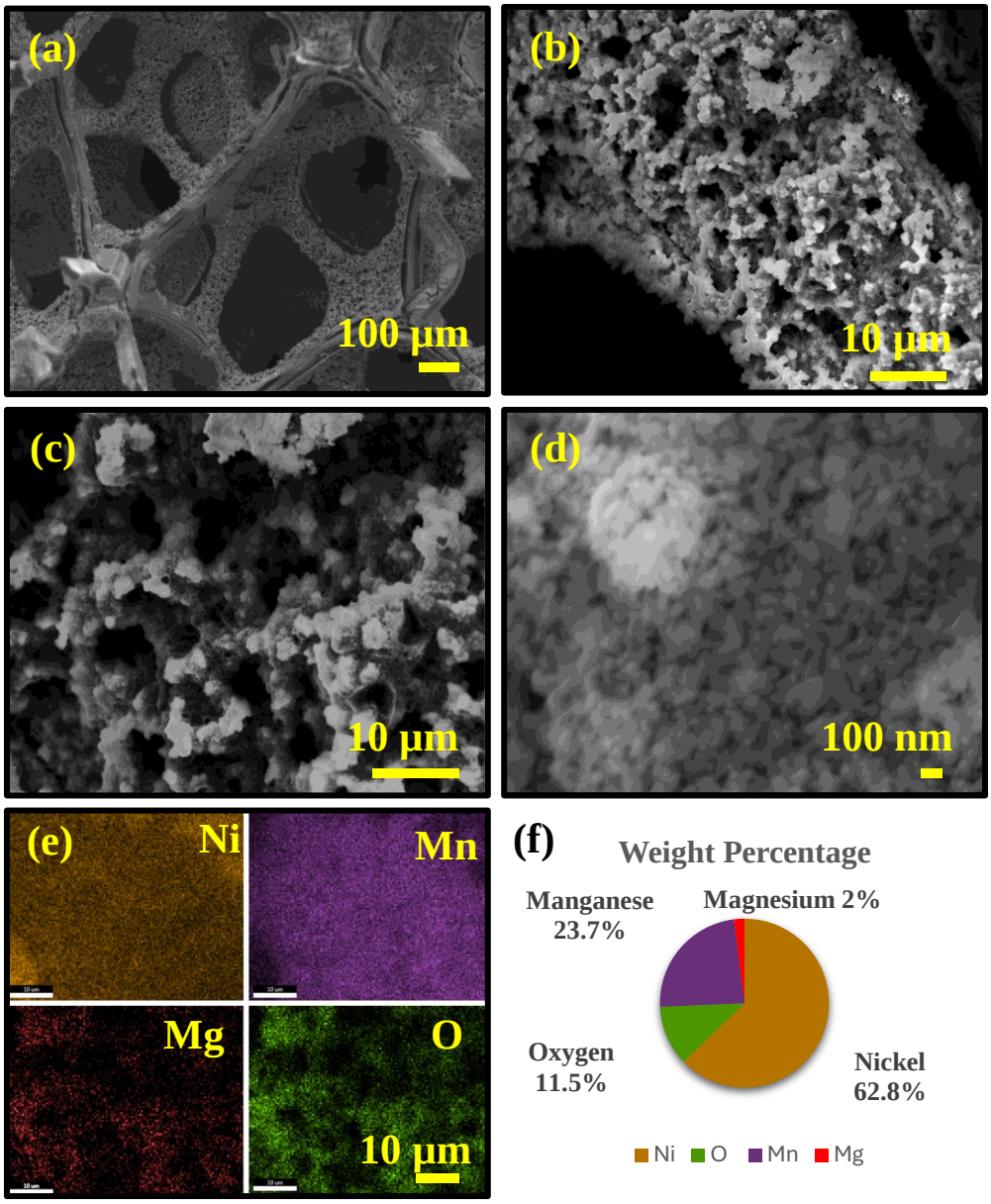

Figure 12. SEM images (a-d) at different magnifications, (e) EDS elemental mapping and (f) weight percentage of Mg2-Mn23.7-Ox/NiF

The manganese oxide (Mn-Ox) was modified with magnesium after its initial deposition to achieve a uniform distribution of the oxide. This modification decreased the surface granularity, resulting in an enhanced overall surface area. Figures 12(a-d) revealed a distinctive coral reef-like structure on the electrode surface, while Figures 12(e-f) indicate that the Mn-Ox distribution has improved, with magnesium aiding in the spread of Mn-Ox over the substrate. Since the magnesium content is at 2%, it may integrate into the lattice structure of Mn-Ox, as suggested by the XRD results. Whereas the manganese content is 23.7%. The SEM images show a more compact surface structure at lower magnesium concentrations.

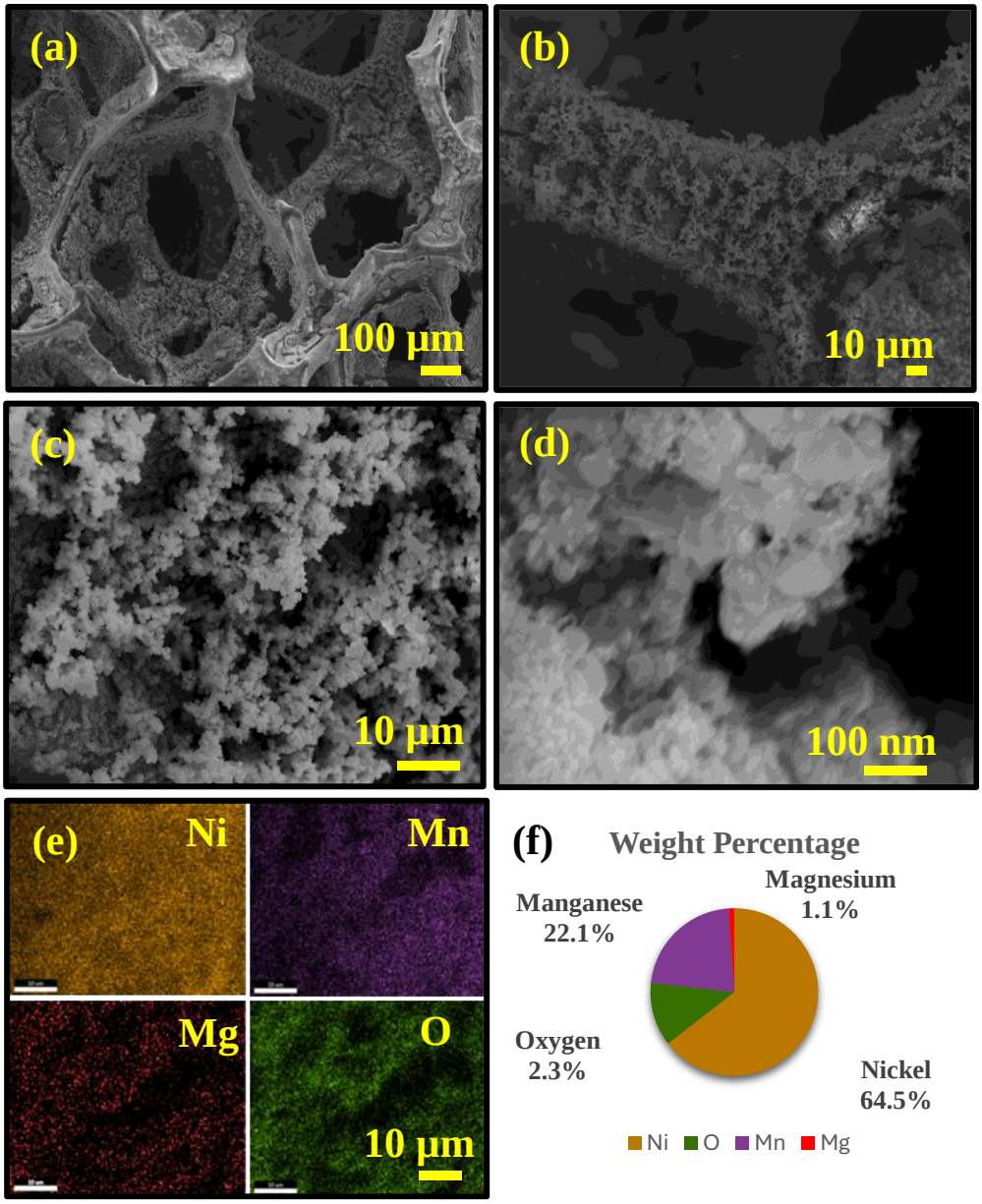

Figure 13. SEM images (a-d) at different magnifications, (e) EDS mapping and (f) weight percentage of Mg1.1-Mn22.1-Ox/NiF

The SEM images (Figure 13(a-d)) show highly uniform structures resembling a coral reef. Elemental analysis (Figure 13(e-f)) indicates a consistent distribution of manganese (Mn) and magnesium (Mg) within the porous nickel foam, with Mg and Mn percentages measured at 1.1% and 22.1%, respectively. This distribution may enhance effective charge and mass transfer during electrochemical evaluations. Comparing the XRD results suggests that Ni_6MnO_8 primarily forms during the calcination process. Therefore, it can be inferred that the observed denser and more uniform layer is attributed to the manganese catalyst, with magnesium aiding in the growth of the manganese oxide layer.

4.2 Electrochemical performance analysis

Electrochemical analysis of the samples is conducted by a potentiostat using linear sweep voltammetry (LSV), cyclic voltammetry (CV), chronoamperometry (CA), electrochemical impedance spectroscopy (EIS) techniques in a customized H-type cell.

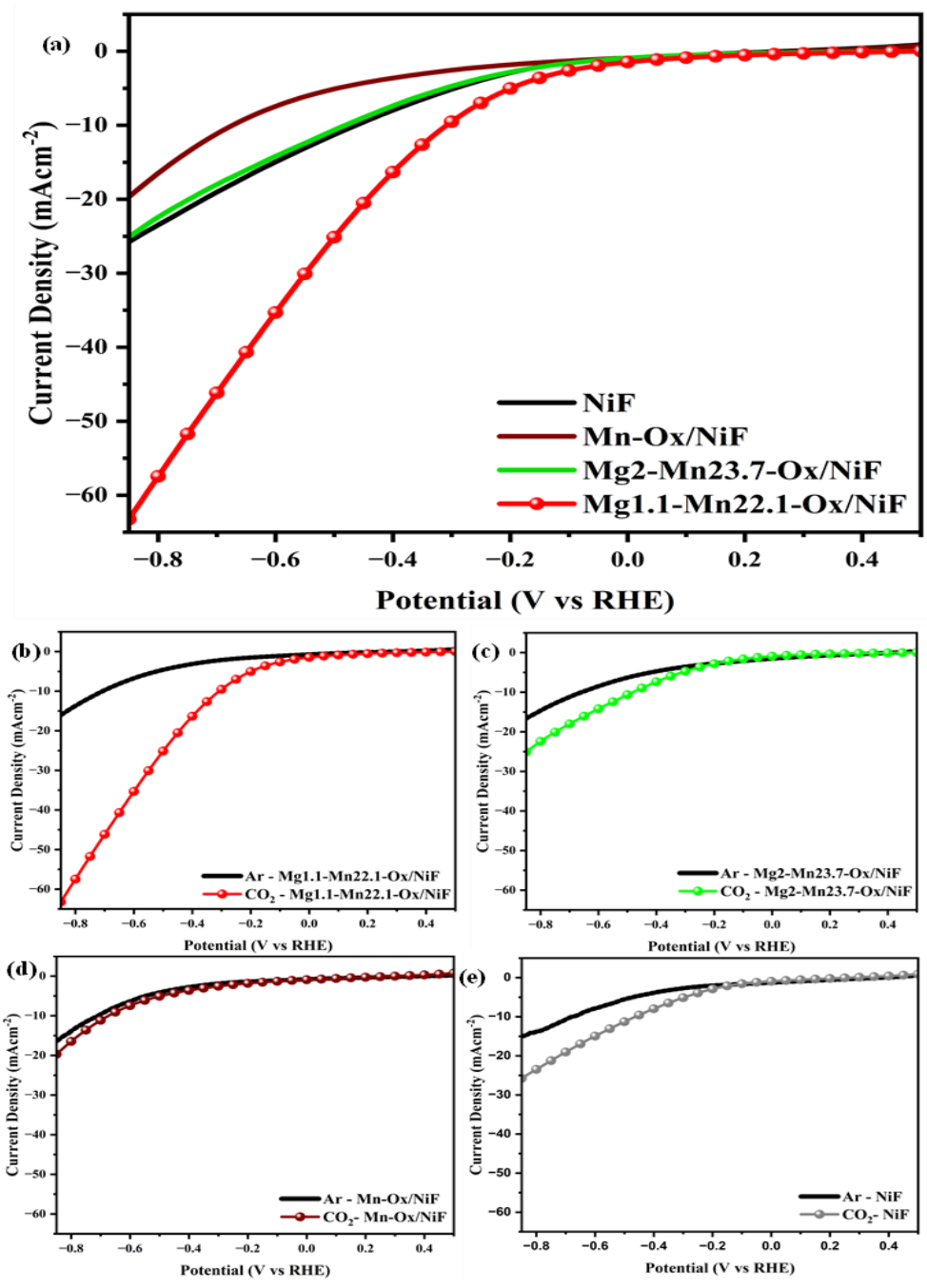

Figure 14. Linear sweep voltammetry curve of (a) Mg1.1-Mn22.1-Ox/NiF, Mg2-Mn23.7-Ox/NiF, Mn-Ox/NiF and NiF in CO_2 saturated medium, (b) Mg1.1-Mn22.1-Ox/NiF, (c) Mg2-Mn23.7-Ox/NiF, (d) Mn-Ox/NiF (e) NiF comparing in Ar and CO_2 saturated medium in 0.5 M NaHCO3 electrolyte in 3 electrode system at scan rate of 5 mV/sec

4.2.1 Linear sweep voltammetry analysis

The characterized electrocatalytic performance of Mg1.1-Mn22.1-Ox/NiF, Mg2-Mn23.7-Ox/NiF, Mn-Ox/NiF and NiF for electrochemical CO_2 reduction was assessed on a working electrode in 0.5 M $NaHCO_3$ aqueous electrolyte in a 3 electrode system. For all samples, linear sweep voltammetry was primarily carried out to assess the response of current density versus applied potential at a scan rate of 5 mV/s as shown in Figure 14(a). This technique was carried out in Ar and CO_2 saturated electrolytic medium. Two gases were purged separately about 1 hour before conducting experiment. The high current density shown in the CO_2 atmosphere is assigned to the accessibility of more active sites in catalysts, which increases overall performance as compared to other catalysts. This technique was carried out in Ar and CO_2 separately in a saturated electrolytic medium for about 1 hour and the CO_2 gas was constantly purged into the electrolytic medium. The behaviour of four samples has been demonstrated in the potential range of 0.5 V to -0.85 V vs RHE under saturated Ar followed by CO_2. Among all the samples, Mg1.1-Mn22.1-Ox/NiF is having a highest current density of -63.24 $mAcm^{-2}$ at -0.85 V vs RHE and lowest onset potential of 0.07 V vs RHE (Figure 14(b)). The same sample with saturated Ar having a current density of -16.01 $mAcm^{-2}$ at -0.85 V vs RHE, confirmed the reduction of CO_2. In case of Mg2-Mn23.7-Ox/NiF (Figure 14(c)), the current density is -25.1 $mAcm^{-2}$ at -0.85 V vs RHE and onset potential is 0.36 V vs RHE in CO_2 medium and in saturated Ar, current density is -16.62 $mAcm^{-2}$. We can see that modifications in the composition and structural arrangement of Mn and Mg oxide might have an impact on electrochemical activity since the ratio and distribution of these components affect overall performance. However, in Figure 14(d), Mn-Ox/NiF shows a current density of –19.69 $mAcm^{-2}$ at −0.85 V vs RHE and onset potential is -0.03 V vs RHE. As NiF has a porous nature, the current density for this sample found as -25.77 $mAcm^{-2}$ at -0.85 V vs RHE in Figure 14(e). As per the obtained LSV results, the Mg1.1-Mn22.1-Ox/NiF catalyst illustrates better current density compared to other prepared catalysts with low overpotential and good onset potential. This is probably due to the presence of active sites in the sample allowing the phenomenon of movable electron which is crucial in improving current density, lower onset potential and lower overpotential.

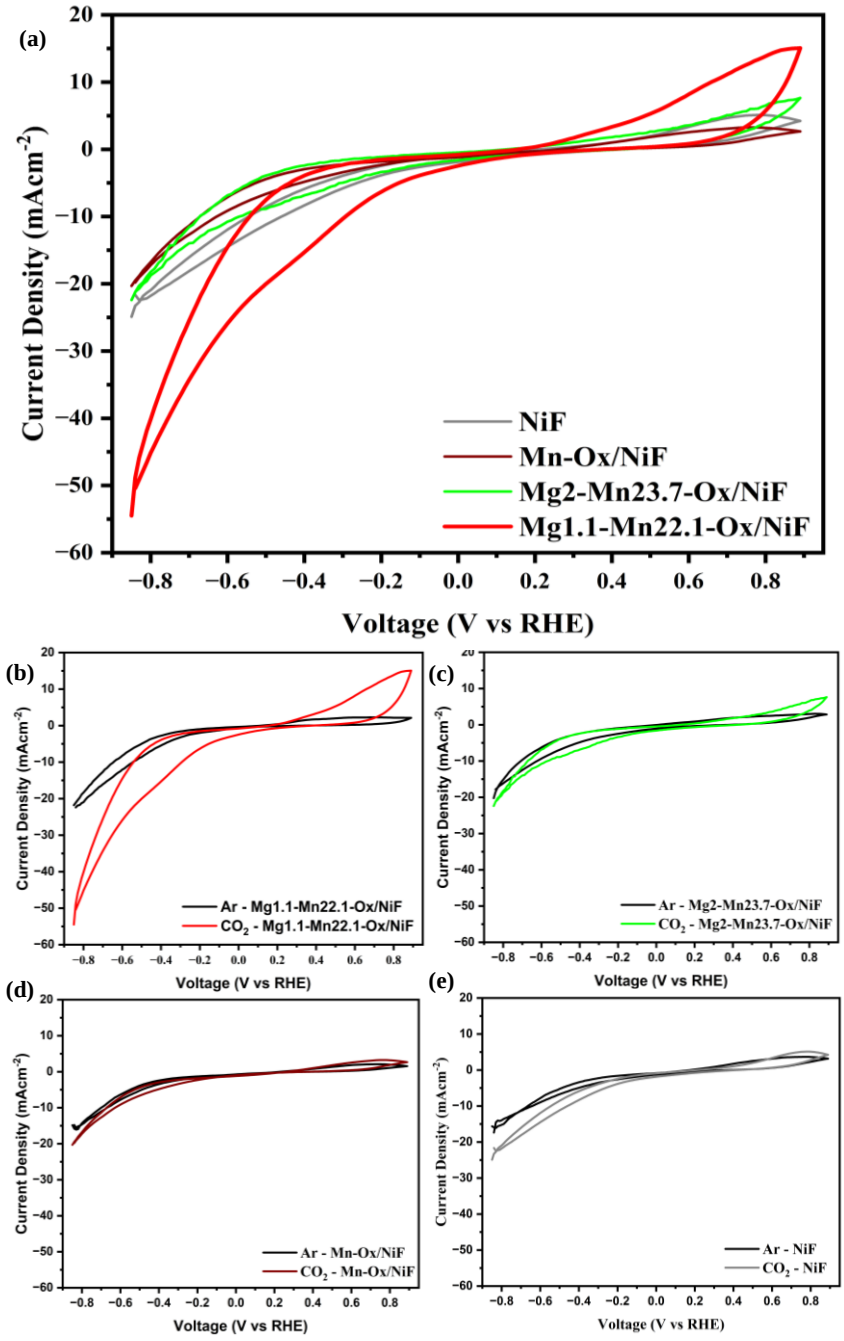

Figure 15. Cyclic voltammetry curve of (a) Mg1.1-Mn22.1-Ox/NiF, Mg2-Mn23.7-Ox/NiF, Mn-Ox/NiF and NiF in CO_2 saturated medium, (b) Mg1.1-Mn22.1-Ox/NiF, (c) Mg2-Mn23.7-Ox/NiF, (d) Mn-Ox/NiF (e) NiF comparing in Ar and CO_2 saturated medium in 0.5 M $NaHCO_3$ electrolyte in 3 electrode system at scan rate of 5 mV/sec

4.2.2 Cyclic voltammetry analysis

Cyclic voltammetry analysis was introduced further to examine the electrocatalytic activity i.e. study the effect of the presence of CO_2 of the samples in the range of 0.89 V to -0.85 V vs RHE at a scan rate of 5 mV/s. The 0.5 M $NaHCO_3$ electrolyte was saturated with Ar and CO_2 separately for about 1 hour before the examination. As seen from the Figure 15(a), Mg1.1-Mn22.1-Ox/NiF exhibited higher current density values than the other samples. Mg1.1-Mn22.1-Ox/NiF showed a higher current density of -54.49 $mAcm^{-2}$ at -0.85 V vs RHE in the CO_2 saturated medium shown in Figure 15(b). It is obvious that the cause for the higher current density means the more intensification reduction of CO_2 in the CO_2 saturated environment [63]. The current density of Mg1.1-Mn22.1-Ox/NiF decreased in case of Ar saturated medium. It was about -21.82 $mAcm^{-2}$ at -0.85 V vs RHE. It might happen due to the hydrogen evolution reaction as no CO_2 was purged and reducted during that time [64]. In terms of the sample Mg2-Mn23.7-Ox/NiF, the current density was -22.41 $mAcm^{-2}$ at -0.85 V vs RHE in CO_2 saturated medium and -20.25 $mAcm^{-2}$ at -0.85 V vs RHE in Ar saturated medium (Figure 15(c). The Mn-Ox/NiF sample drew a current density of about -20.32 $mAcm^{-2}$ at -0.85 V vs RHE in CO_2 saturated medium and -15.80 mAcm-2 at -0.85 V vs RHE (Figure 15(d)). Lastly, current density of NiF was -24.92 $mAcm^{-2}$ at -0.85 V vs RHE in CO_2 saturated situation whereas it was -15.64 $mAcm^{-2}$ at -0.85 V vs RHE in Ar saturated medium (Figure 15(e)). By observing the value of current density, it can be stated that the system was in relation to the value in linear sweep voltammetry.

4.3.3 Chronoamperometry analysis

The electrolytic activities of prepared electrocatalysts were evaluated again by chronoamperometry technique. It is a technique where a constant potential is applied, and the current is monitored as a function of time to investigate the stability. First of all, this technique was applied to validate the value getting from linear sweep voltammetry and cyclic voltammetry at -0.85 V vs RHE for 120 seconds. From Figure 16(a), it is clearly observed that Mg1.1-Mn22.1-Ox/NiF gained the higher current density not only this time but also in the earlier techniques in this work. The average current density was -22.82 $mAcm^{-2}$, -19.31 $mAcm^{-2}$, -19.76 $mAcm^{-2}$, -23.35 $mAcm^{-2}$, -46.45 $mAcm^{-2}$ for our samples NiF, Mn-Ox/NiF, Mg2-Mn23.7-Ox/NiF, Mg1.1-Mn22.1-Ox/NiF respectively in the CO_2 saturated medium. On the contrary, the average current density was -14.77 $mAcm^{-2}$, -14.9 $mAcm^{-2}$, -15.82 $mAcm^{-2}$, -19.67 $mAcm^{-2}$ for the NiF, Mn-Ox/NiF, Mg2-Mn23.7-Ox/NiF, Mg1.1-Mn22.1-Ox/NiF respectively (Figure 16(b-f). The value which we were getting from the electrochemical techniques was close enough to validate the system. After evaluating the system and seeing the performance of all the electrocatalysts, Mg1.1-Mn22.1-Ox/NiF was selected for further test to conduct the stability test by chronoamperometry technique and getting the following product information.

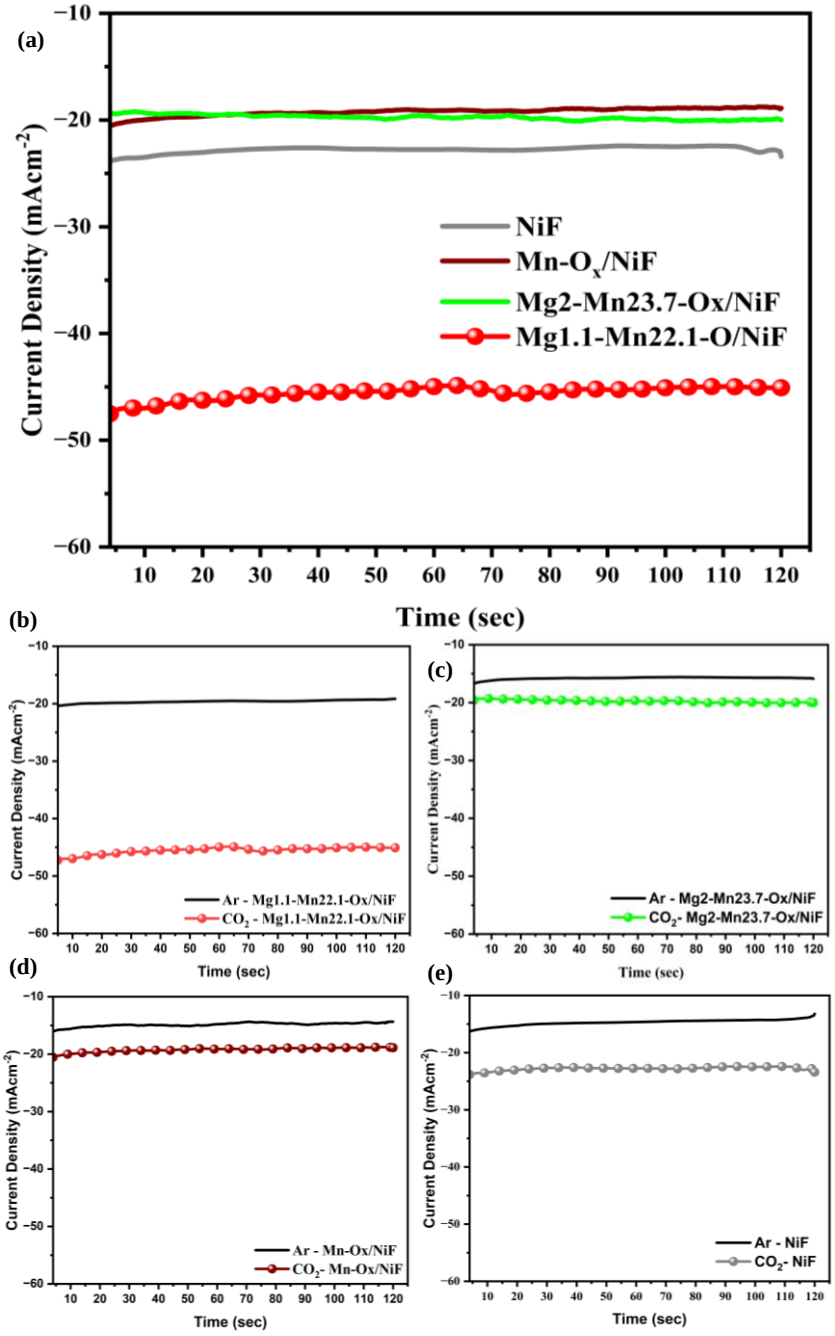

Figure 16. Chronoamperometry curve of (a) Mg1.1-Mn22.1-O_x/NiF, Mg2-Mn23.7-Ox/NiF, Mn-Ox/NiF and NiF in CO_2 saturated medium, (b) Mg1.1-Mn22.1-Ox/NiF, (c) Mg2-Mn23.7-Ox/NiF, (d) Mn-Ox/NiF (e) NiF comparing in Ar and CO_2 saturated medium in 0.5 M $NaHCO_3$ electrolyte in 3 electrode system At -0.85 V vs RHE for 120 sec

4.3 Product analysis

The stability of synthesized Mg1.1-Mn22.1-Ox/NiF was examined through chronoamperometry analysis at -0.85 V vs RHE for about 22 hours. Initially, the electrolyte was bubbled with CO_2 before 2 hours from the experiment. Only Mg1.1-Mn22.1-Ox/NiF electrocatalyst was selected for this test after comparing the overall higher performance in Linear sweep voltammetry, Cyclic voltammetry and chronoamperometry test. The main reason is activity along with thinking the synergistic activities between the components, the bimetallic catalysts' active surface area which can promote the adsorption of intermediates during the formation of formate. The FTIR spectra of formate is shown in Figure 17. The bands at 1761 and 1060 cm^{-1} are ascribed to the C = O and C–O stretching vibrations of carboxylic acid group, respectively [65]. Furthermore, the doublet bands at 1641 and 1357 cm^{-1} correspond to the $COOH^-$ symmetric and asymmertric vibrations [66]. The doublet bands at 2922 and 2849 cm^{-1} in the FTIR spectrum are assigned to the C-H stretching vibrations [67]. The broad band ranging from 3000 to 3600 cm^{-1} with peak centered at 3328 cm^{-1} is attributed to the O–H stretching vibrations of adsorbed water molecules.

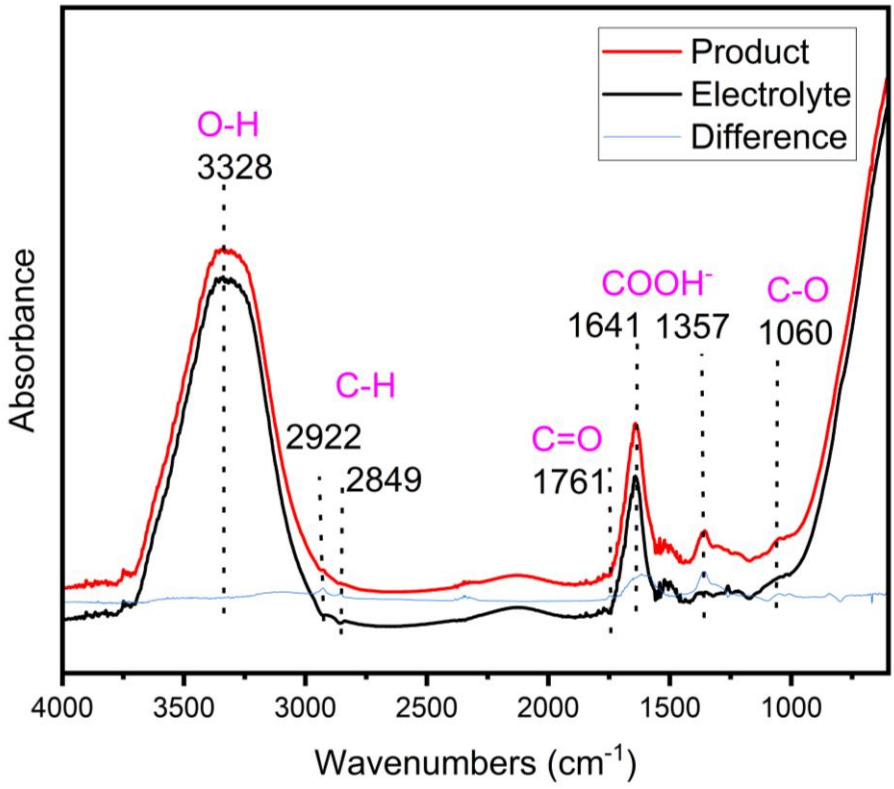

Figure 17. FTIR spectra analysis of the product

Chapter 5

Conclusion

In this study, magnesium-manganese-based oxides were successfully synthesized and directly grown on nickel foam as a substrate. These materials were employed as catalysts for electrochemical CO_2 reduction (CO_2RR). The catalysts were prepared by immersing nickel foam completely into a solution, enabling the formation of magnesium-manganese oxides on the nickel surface. To characterize the catalysts, a comprehensive set of analytical and spectroscopic techniques, including X-ray diffraction (XRD), scanning electron microscopy (SEM), and energy-dispersive X-ray spectroscopy (EDS), was utilized. These investigations confirmed that the Mg1.1-Mn22.1-Ox/NiF catalyst, synthesized with a molar concentration ratio of 0.5:1 (Mg:Mn), exhibited high crystallinity for manganese. Magnesium was found to play a key role in enhancing the catalytic performance during electrochemical testing.
The unique coral-reef-like structure of magnesium-manganese oxides grown on nickel foam was considered a critical factor in improving charge and electron transfer efficiency, ultimately enhancing the overall catalytic activity. Electrochemical testing demonstrated that the catalyst achieved a remarkable current density of -63.24 mA cm^{-2} at an applied potential of -0.85 V vs. RHE. Additionally, the catalyst exhibited an exceptionally low onset potential of approximately 0.07 V, indicating faster reaction kinetics and superior catalytic efficiency. These findings highlight the promising potential of magnesium-manganese-based oxides for CO_2 reduction, paving the way for future research into further optimizing the catalyst structure and composition. The results provide a strong foundation for developing advanced electrocatalysts with high activity, stability, and efficiency for CO_2RR.

Recommendation

The aim of this study was to design highly active manganese-based oxide on nickel foam for electrochemical CO_2 reduction to formate. The aim will be achieved more successfully through the following.

1. Optimization of Catalysts: Future research may concentrate on refining the composition and molar ratios of magnesium and manganese to further improve catalytic activity, selectivity, and stability. Investigating doping with alternative metals or non-metals may reveal further synergistic effects.
2. Alternative Substrates: Examine the application of alternative conductive substrates with diverse surface morphologies and characteristics, such carbon-based materials or metal-organic frameworks, to improve electron transfer and CO_2 adsorption.
3. Comprehensive Mechanistic Investigations: Utilize sophisticated in-situ characterisation methods, like in-situ Raman spectroscopy or in-situ X-ray absorption spectroscopy, to obtain enhanced understanding of the reaction processes and the function of magnesium in the catalytic process.
4. Scalability and Industrial Feasibility: Assess the scalability of the catalyst synthesis process and its efficacy under industrial conditions, including flow cell designs, to determine its viability for practical CO_2 reduction applications.
5. Expanded Product Range: Examine the catalyst's capacity for generating multi-carbon products through the alteration of reaction parameters or integration with alternative catalytic systems, hence enhancing its applicability.
6. Long-Term Stability Assessment: Conduct long-term stability assessments under diverse electrochemical circumstances to verify consistent performance and durability throughout prolonged operational durations.

List of References

[1] M. R. Allen *et al.*, "Net Zero: Science, Origins, and Implications," *Annu. Rev. Environ. Resour.*, vol. 47, no. 1, pp. 849–887, Oct. 2022, doi: 10.1146/annurev-environ-112320-105050.

[2] K. Akimoto, F. Sano, J. Oda, H. Kanaboshi, and Y. Nakano, "Climate change mitigation measures for global net-zero emissions and the roles of CO2 capture and utilization and direct air capture," *Energy Clim. Change*, vol. 2, p. 100057, Dec. 2021, doi: 10.1016/j.egycc.2021.100057.

[3] E. Alper and O. Yuksel Orhan, "CO2 utilization: Developments in conversion processes," *Petroleum*, vol. 3, no. 1, pp. 109–126, Mar. 2017, doi: 10.1016/j.petlm.2016.11.003.

[4] J. Hansen *et al.*, "Ice melt, sea level rise and superstorms: evidence from paleoclimate data, climate modeling, and modern observations that 2 °C global warming is highly dangerous," Jul. 23, 2015, *Dynamics/Atmospheric Modelling/Troposphere/Physics (physical properties and processes)*. doi: 10.5194/acpd-15-20059-2015.

[5] X. Li, A. Ulfat, Z. Lv, L. Fang, D. Jiang, and F. Liu, "Effect of multigenerational exposure to elevated atmospheric CO2 concentration on grain quality in wheat," *Environ. Exp. Bot.*, vol. 157, pp. 310–319, Jan. 2019, doi: 10.1016/j.envexpbot.2018.10.028.

[6] L. J. R. Nunes, "The Rising Threat of Atmospheric CO2: A Review on the Causes, Impacts, and Mitigation Strategies," *Environments*, vol. 10, no. 4, p. 66, Apr. 2023, doi: 10.3390/environments10040066.

[7] Q. Li, Y.-N. Wei, and Z.-A. Chen, "Water-CCUS nexus: challenges and opportunities of China's coal chemical industry," *Clean Technol. Environ. Policy*, vol. 18, no. 3, pp. 775–786, Mar. 2016, doi: 10.1007/s10098-015-1049-z.

[8] H.-R. "Molly" Jhong, S. Ma, and P. J. Kenis, "Electrochemical conversion of CO2 to useful chemicals: current status, remaining challenges, and future opportunities," *Curr. Opin. Chem. Eng.*, vol. 2, no. 2, pp. 191–199, May 2013, doi: 10.1016/j.coche.2013.03.005.

[9] D. Pakhare and J. Spivey, "A review of dry (CO_2) reforming of methane over noble metal catalysts," *Chem Soc Rev*, vol. 43, no. 22, pp. 7813–7837, Feb. 2014, doi: 10.1039/C3CS60395D.

[10] V. Romanov, Y. Soong, C. Carney, G. E. Rush, B. Nielsen, and W. O'Connor, "Mineralization of Carbon Dioxide: A Literature Review," *ChemBioEng Rev.*, vol. 2, no. 4, pp. 231–256, Aug. 2015, doi: 10.1002/cben.201500002.

[11] W. Wang, S. Wang, X. Ma, and J. Gong, "Recent advances in catalytic hydrogenation of carbon dioxide," *Chem. Soc. Rev.*, vol. 40, no. 7, p. 3703, 2011, doi: 10.1039/c1cs15008a.

[12] P. M. Schenk *et al.*, "Second Generation Biofuels: High-Efficiency Microalgae for Biodiesel Production," *BioEnergy Res.*, vol. 1, no. 1, pp. 20–43, Mar. 2008, doi: 10.1007/s12155-008-9008-8.

[13] Y. Izumi, "Recent advances in the photocatalytic conversion of carbon dioxide to fuels with water and/or hydrogen using solar energy and beyond," *Coord. Chem. Rev.*, vol. 257, no. 1, pp. 171–186, Jan. 2013, doi: 10.1016/j.ccr.2012.04.018.

[14] J. F. De La Fuente, S. H. Moreno, A. I. Stankiewicz, and G. D. Stefanidis, "Reduction of CO2 with hydrogen in a non-equilibrium microwave plasma reactor," *Int. J. Hydrog. Energy*, vol. 41, no. 46, pp. 21067–21077, Dec. 2016, doi: 10.1016/j.ijhydene.2016.08.032.

[15] S. Verma, B. Kim, H. "Molly" Jhong, S. Ma, and P. J. A. Kenis, "A Gross-Margin Model for Defining Technoeconomic Benchmarks in the Electroreduction of CO_2," *ChemSusChem*, vol. 9, no. 15, pp. 1972–1979, Aug. 2016, doi: 10.1002/cssc.201600394.

[16] A. Dindi, D. V. Quang, L. F. Vega, E. Nashef, and M. R. M. Abu-Zahra, "Applications of fly ash for CO2 capture, utilization, and storage," *J. CO2 Util.*, vol. 29, pp. 82–102, Jan. 2019, doi: 10.1016/j.jcou.2018.11.011.

[17] M. Jouny, W. Luc, and F. Jiao, "General Techno-Economic Analysis of CO_2 Electrolysis Systems," *Ind. Eng. Chem. Res.*, vol. 57, no. 6, pp. 2165–2177, Feb. 2018, doi: 10.1021/acs.iecr.7b03514.

[18] Y. Yang, S. Ajmal, X. Zheng, and L. Zhang, "Efficient nanomaterials for harvesting clean fuels from electrochemical and photoelectrochemical CO_2 reduction," *Sustain. Energy Fuels*, vol. 2, no. 3, pp. 510–537, 2018, doi: 10.1039/C7SE00371D.

[19] J. Eppinger and K.-W. Huang, "Formic Acid as a Hydrogen Energy Carrier," *ACS Energy Lett.*, vol. 2, no. 1, pp. 188–195, Jan. 2017, doi: 10.1021/acsenergylett.6b00574.

[20] C. Muhire, A. Tesfay Reda, D. Zhang, X. Xu, and C. Cui, "An overview on metal Oxide-based materials for iodine capture and storage," *Chem. Eng. J.*, vol. 431, p. 133816, Mar. 2022, doi: 10.1016/j.cej.2021.133816.

[21] R.-L. Zhang *et al.*, "Straw-like phosphorus-doped Co2MnO4 nanoneedle arrays supported on nickel foam for high-efficiency hydrogen evolution reaction in wide pH range of electrolytes," *Appl. Surf. Sci.*, vol. 548, p. 149280, May 2021, doi: 10.1016/j.apsusc.2021.149280.

[22] D. Gao *et al.*, "Size-Dependent Electrocatalytic Reduction of CO_2 over Pd Nanoparticles," *J. Am. Chem. Soc.*, vol. 137, no. 13, pp. 4288–4291, Apr. 2015, doi: 10.1021/jacs.5b00046.

[23] C. Kim *et al.*, "Achieving Selective and Efficient Electrocatalytic Activity for CO_2 Reduction Using Immobilized Silver Nanoparticles," *J. Am. Chem. Soc.*, vol. 137, no. 43, pp. 13844–13850, Nov. 2015, doi: 10.1021/jacs.5b06568.

[24] C. Rogers, W. S. Perkins, G. Veber, T. E. Williams, R. R. Cloke, and F. R. Fischer, "Synergistic Enhancement of Electrocatalytic CO_2 Reduction with Gold Nanoparticles Embedded in Functional Graphene Nanoribbon Composite Electrodes," *J. Am. Chem. Soc.*, vol. 139, no. 11, pp. 4052–4061, Mar. 2017, doi: 10.1021/jacs.6b12217.

[25] B. Zhang *et al.*, "Manganese acting as a high-performance heterogeneous electrocatalyst in carbon dioxide reduction," *Nat. Commun.*, vol. 10, no. 1, p. 2980, Jul. 2019, doi: 10.1038/s41467-019-10854-1.

[26] M. Bourrez, F. Molton, S. Chardon-Noblat, and A. Deronzier, "[Mn(bipyridyl)$(CO)_3$ Br]: An Abundant Metal Carbonyl Complex as Efficient Electrocatalyst for CO_2 Reduction," *Angew. Chem.*, vol. 123, no. 42, pp. 10077–10080, Oct. 2011, doi: 10.1002/ange.201103616.

[27] Z. Abdi *et al.*, "In Situ Synthesis of Manganese Oxide as an Oxygen-Evolving Catalyst: A New Strategy," *Chem. – Eur. J.*, vol. 27, no. 4, pp. 1330–1336, Jan. 2021, doi: 10.1002/chem.202002942.

[28] T. Li *et al.*, "Loading CuO on the surface of MgO with low-coordination basic O2– sites for effective enhanced CO2 capture and photothermal synergistic catalytic reduction of CO2 to ethanol," *Chin. J. Chem. Eng.*, vol. 61, pp. 58–67, Sep. 2023, doi: 10.1016/j.cjche.2023.03.008.

[29] A. Arab, Z. Sktani, Q. Zhou, Z. Ahmad, and P. Chen, "Effect of MgO Addition on the Mechanical and Dynamic Properties of Zirconia Toughened Alumina (ZTA) Ceramics," *Materials*, vol. 12, no. 15, p. 2440, Jul. 2019, doi: 10.3390/ma12152440.

[30] L. -P. Lefebvre, J. Banhart, and D. C. Dunand, "Porous Metals and Metallic Foams: Current Status and Recent Developments," *Adv. Eng. Mater.*, vol. 10, no. 9, pp. 775–787, Sep. 2008, doi: 10.1002/adem.200800241.

[31] C. Guan *et al.*, "Hybrid structure of cobalt monoxide nanowire @ nickel hydroxidenitrate nanoflake aligned on nickel foam for high-rate supercapacitor," *Energy Environ. Sci.*, vol. 4, no. 11, p. 4496, 2011, doi: 10.1039/c1ee01685g.

[32] W. Leitner, "The coordination chemistry of carbon dioxide and its relevance for catalysis: a critical survey," *Coord. Chem. Rev.*, vol. 153, pp. 257–284, Aug. 1996, doi: 10.1016/0010-8545(95)01226-5.

[33] L. Yoon Suk Lee and K.-Y. Wong, "Electrocatalytic Reduction of Carbon Dioxide," *Chem*, vol. 3, no. 5, pp. 717–718, Nov. 2017, doi: 10.1016/j.chempr.2017.09.018.

[34] A. M. Appel *et al.*, "Frontiers, Opportunities, and Challenges in Biochemical and Chemical Catalysis of CO_2 Fixation," *Chem. Rev.*, vol. 113, no. 8, pp. 6621–6658, Aug. 2013, doi: 10.1021/cr300463y.

[35] A. R. Woldu, Z. Huang, P. Zhao, L. Hu, and D. Astruc, "Electrochemical CO2 reduction (CO2RR) to multi-carbon products over copper-based catalysts," *Coord. Chem. Rev.*, vol. 454, p. 214340, Mar. 2022, doi: 10.1016/j.ccr.2021.214340.

[36] R. Kas, K. Yang, D. Bohra, R. Kortlever, T. Burdyny, and W. A. Smith, "Electrochemical CO_2 reduction on nanostructured metal electrodes: fact or defect?," *Chem. Sci.*, vol. 11, no. 7, pp. 1738–1749, 2020, doi: 10.1039/C9SC05375A.

[37] K. P. Kuhl, E. R. Cave, D. N. Abram, and T. F. Jaramillo, "New insights into the electrochemical reduction of carbon dioxide on metallic copper surfaces," *Energy Environ. Sci.*, vol. 5, no. 5, p. 7050, 2012, doi: 10.1039/c2ee21234j.

[38] G. Leonzio, A. Hankin, and N. Shah, "CO2 electrochemical reduction: A state-of-the-art review with economic and environmental analyses," *Chem. Eng. Res. Des.*, vol. 208, pp. 934–955, Aug. 2024, doi: 10.1016/j.cherd.2024.07.014.

[39] Y. Matsubara, D. C. Grills, and Y. Kuwahara, "Thermodynamic Aspects of Electrocatalytic CO_2 Reduction in Acetonitrile and with an Ionic Liquid as Solvent or Electrolyte," *ACS Catal.*, vol. 5, no. 11, pp. 6440–6452, Nov. 2015, doi: 10.1021/acscatal.5b00656.

[40] S. Xu and E. A. Carter, "Theoretical Insights into Heterogeneous (Photo)electrochemical CO_2 Reduction," *Chem. Rev.*, vol. 119, no. 11, pp. 6631–6669, Jun. 2019, doi: 10.1021/acs.chemrev.8b00481.

[41] A. A. Bunaciu, E. G. Udriştioiu, and H. Y. Aboul-Enein, "X-Ray Diffraction: Instrumentation and Applications," *Crit. Rev. Anal. Chem.*, vol. 45, no. 4, pp. 289–299, Oct. 2015, doi: 10.1080/10408347.2014.949616.

[42] S. Tsiper, O. Dicker, I. Kaizerman, Z. Zohar, M. Segev, and Y. C. Eldar, "Sparsity-Based Super Resolution for SEM Images," *Nano Lett.*, vol. 17, no. 9, pp. 5437–5445, Sep. 2017, doi: 10.1021/acs.nanolett.7b02091.

[43] R. M. Tromp, "Energy-dispersive X-ray spectroscopy in a low energy electron microscope," *Ultramicroscopy*, vol. 259, p. 113935, May 2024, doi: 10.1016/j.ultramic.2024.113935.

[44] A. Sengeni, "How reliable are the overpotentials reported in energy conversion electrocatalysis?," *Catal. Sci. Technol.*, vol. 14, no. 8, pp. 2025–2039, 2024, doi: 10.1039/D4CY00079J.

[45] G. Bontempelli and R. Toniolo, "VOLTAMMETRY | Linear Sweep and Cyclic," in *Encyclopedia of Analytical Science*, Elsevier, 2005, pp. 188–197. doi: 10.1016/B0-12-369397-7/00647-6.

[46] J. H. Brown, "Development and Use of a Cyclic Voltammetry Simulator To Introduce Undergraduate Students to Electrochemical Simulations," *J. Chem. Educ.*, vol. 92, no. 9, pp. 1490–1496, Sep. 2015, doi: 10.1021/acs.jchemed.5b00225.

[47] E. Núñez-Bajo and M. T. Fernández Abedul, "Chronoamperometric determination of ascorbic acid on paper-based devices," in *Laboratory Methods in Dynamic Electroanalysis*, Elsevier, 2020, pp. 75–83. doi: 10.1016/B978-0-12-815932-3.00008-5.

[48] R. Kula, M. Bébarová, P. Matejovič, J. Šimurda, and M. Pásek, "Current density as routine parameter for description of ionic membrane current: is it always the best option?," *Prog. Biophys. Mol. Biol.*, vol. 157, pp. 24–32, Nov. 2020, doi: 10.1016/j.pbiomolbio.2019.11.011.

[49] C. Batchelor-McAuley, "Defining the onset potential," *Curr. Opin. Electrochem.*, vol. 37, p. 101176, Feb. 2023, doi: 10.1016/j.coelec.2022.101176.

[50] S. Panero, "ELECTROCHEMICAL THEORY | Kinetics," in *Encyclopedia of Electrochemical Power Sources*, Elsevier, 2009, pp. 14–22. doi: 10.1016/B978-044452745-5.00034-4.

[51] Y. Yang and F. Li, "Reactor design for electrochemical CO2 conversion toward large-scale applications," *Curr. Opin. Green Sustain. Chem.*, vol. 27, p. 100419, Feb. 2021, doi: 10.1016/j.cogsc.2020.100419.

[52] S. Liang, N. Altaf, L. Huang, Y. Gao, and Q. Wang, "Electrolytic cell design for electrochemical CO2 reduction," *J. CO2 Util.*, vol. 35, pp. 90–105, Jan. 2020, doi: 10.1016/j.jcou.2019.09.007.

[53] C. Zhao and J. Wang, "Electrochemical reduction of CO2 to formate in aqueous solution using electro-deposited Sn catalysts," *Chem. Eng. J.*, vol. 293, pp. 161–170, Jun. 2016, doi: 10.1016/j.cej.2016.02.084.

[54] C. Costentin, M. Robert, and J.-M. Savéant, "Catalysis of the electrochemical reduction of carbon dioxide," *Chem Soc Rev*, vol. 42, no. 6, pp. 2423–2436, 2013, doi: 10.1039/C2CS35360A.

[55] L. -P. Lefebvre, J. Banhart, and D. C. Dunand, "Porous Metals and Metallic Foams: Current Status and Recent Developments," *Adv. Eng. Mater.*, vol. 10, no. 9, pp. 775–787, Sep. 2008, doi: 10.1002/adem.200800241.

[56] J. Zhang, W. Sun, L. Ding, Z. Wu, and F. Gao, "Au Nanocrystals@Defective Amorphous MnO_2 Nanosheets Core/Shell Nanostructure with Effective CO_2 Adsorption and Activation toward CO_2 Electroreduction to CO," *ACS Sustain. Chem. Eng.*, vol. 9, no. 14, pp. 5230–5239, Apr. 2021, doi: 10.1021/acssuschemeng.1c00995.

[57] X. Hu, X. Tian, Y.-W. Lin, and Z. Wang, "Nickel foam and stainless steel mesh as electrocatalysts for hydrogen evolution reaction, oxygen evolution reaction and overall water splitting in alkaline media," *RSC Adv.*, vol. 9, no. 54, pp. 31563–31571, 2019, doi: 10.1039/C9RA07258F.

[58] J.-H. Woo *et al.*, "Effect of the Ni-to-CaO Ratio on Integrated CO2 Capture and Direct Methanation," *Catalysts*, vol. 13, no. 8, p. 1174, Jul. 2023, doi: 10.3390/catal13081174.

[59] A. H. Al-khaykanee, S. R. Ghorbani, H. Arabi, and R. Ghanbari, "NiMnO3-rGO nanocomposites in a cotton-based flexible yarn supercapacitor," *J. Mater. Sci. Mater. Electron.*, vol. 35, no. 2, p. 141, Jan. 2024, doi: 10.1007/s10854-023-11868-8.

[60] J. Hong *et al.*, "Ni_2 Mn-layered double oxide electrodes in organic electrolyte based supercapacitors," *RSC Adv.*, vol. 11, no. 44, pp. 27267–27275, 2021, doi: 10.1039/D1RA04681K.

[61] W. Xu *et al.*, "Less Is More: Selective-Atom-Removal-Derived Defective MnOx Catalyst for Efficient Propane Oxidation," *Nanomaterials*, vol. 14, no. 11, p. 907, May 2024, doi: 10.3390/nano14110907.

[62] H. Zhang, X. Zheng, T. Xu, and P. Zhang, "Atomically Dispersed Y or La on Birnessite-Type MnO_2 for the Catalytic Decomposition of Low-Concentration Toluene at Room Temperature," *ACS Appl. Mater. Interfaces*, vol. 13, no. 15, pp. 17532–17542, Apr. 2021, doi: 10.1021/acsami.1c01433.

[63] W. Lv, R. Zhang, P. Gao, and L. Lei, "Studies on the faradaic efficiency for electrochemical reduction of carbon dioxide to formate on tin electrode," *J. Power Sources*, vol. 253, pp. 276–281, May 2014, doi: 10.1016/j.jpowsour.2013.12.063.

[64] K. Zhang and S.-S. Park, "Effects of current density on anodizing behavior, micro-structure, and electrical properties of ZrO2-coated Al foils," *Appl. Surf. Sci.*, vol. 477, pp. 44–49, May 2019, doi: 10.1016/j.apsusc.2018.01.119.

[65] J. Liu, H. Bai, Y. Wang, Z. Liu, X. Zhang, and D. D. Sun, "Self-Assembling TiO_2 Nanorods on Large Graphene Oxide Sheets at a Two-Phase Interface and Their Anti-Recombination in Photocatalytic Applications," *Adv. Funct. Mater.*, vol. 20, no. 23, pp. 4175–4181, Dec. 2010, doi: 10.1002/adfm.201001391.

[66] J. G. Zhao and H. H. Zhang, "Hydrothermal synthesis and characterization of ZnS hierarchical microspheres," *Superlattices Microstruct.*, vol. 51, no. 5, pp. 663–667, May 2012, doi: 10.1016/j.spmi.2012.02.004.

[67] M. Nara, H. Torii, and M. Tasumi, "Correlation between the Vibrational Frequencies of the Carboxylate Group and the Types of Its Coordination to a Metal Ion: An *ab Initio* Molecular Orbital Study," *J. Phys. Chem.*, vol. 100, no. 51, pp. 19812–19817, Jan. 1996, doi: 10.1021/jp9615924.

Appendices

<table>
<tr><td>Description of activity</td><td>Participants</td><td>Date</td><td>20.11.2024 – 21.11.2024</td></tr>
<tr><td rowspan="3">Electrochemical CO_2 Reduction using metal oxides
1. Synthesis of Mg-Mn-Ox/Nickel Foam (NiF)
2. Preparation of electrolyte (0.5 M $NaHCO_3$)
3. Electrochemical testing for CO_2 reduction</td><td rowspan="3">Adittya Chowdhury Joy</td><td>Unit</td><td>D2021</td></tr>
<tr><td>SJA-responsible</td><td>Adittya Chowdhury Joy</td></tr>
<tr><td>Does a SOP exist for the activity</td><td>Yes</td></tr>
<tr><td>Task divided into parts
The process is divided into parts and in successive order</td><td>Risk
What are unwanted events that may occur</td><td colspan="2">Preventive measures
Measures that reduces risks and reduces consequences if an unwanted event occurs</td></tr>
<tr><td>Preparation of Materials
1. Required Materials: Manganese (II) Nitrate Tetrahydrate, Magnesium Chloride Hexahydrate, Ethylene Glycol, Formic Acid 98%, Deionized Water, NiF.
2. Add 3 mL EG in H_2O by using pipette or syringe with a fine needle drop by drop slowly in fume hood.
3. Prepare 1M manganese (II) nitrate tetrahydrate and 0.5M Magnesium chloride hexahydrate.</td><td>1. Manganese (II) Nitrate Tetrahydrate is an oxidizer and can cause irritation to skin, eyes, and respiratory. Magnesium Chloride Hexahydrate can also cause irritation. Ethylene Glycol is toxic and can cause damage to organs. Formic Acid (98%) can cause severe burns to the skin and eyes. Nickel foam is metallic, and its sharp edges or thin filaments can cause</td><td colspan="2">1. Always wear gloves, mask, safety goggles, and a lab coat. Work in a fume hood to avoid inhaling vapors. label appropriately with hazard warnings. Keep each chemical in its original container when not in use, and store them in a cool, dry place.
2. Always work in a fume hood and introduce EG in small increments while stirring the solution constantly.
3. Ensure proper PPE and ventilation</td></tr>
</table>

4. Heat the solution. 5. Add 2 mL Formic Acid 98% in the solution by using pipette or syringe with a fine needle drop by drop in fume hood. 6. Add NF to the solution. 7. Heat at 80 degrees.	abrasions when handled. 2. Sudden interaction may cause a rapid temperature rise, which could lead to localized overheating. 3. Cause irritation to skin, eyes, and respiratory system. 4. Stirring too quickly can cause the liquid to splash. 5. Highly corrosive. 6. Nickel foam has sharp edges or thin filaments that can cause cuts. 7. It can release hazardous fumes upon heating.	4. Always use a beaker that is large enough to prevent overflow and splashing. 5. Handle with extreme care in a fume hood, and always wear protective equipment. 6. Handle with proper care. Use proper PPE and tools. 7. Conduct the heating process in a fume hood. Use a temperature-controlled hot plate to avoid overheating. 8. Place all contaminated solid waste and disposable items into designated waste bags. Place any leftover solutions in a designated chemical waste area. Place the used nickel foam in a separate waste container. 9. For cleaning the glass and tools used in the experiment, at first,rinse with water, then use deionized water. Finally, follow with a final rinse of acetone or ethanol or iso-propanol to remove any residual.

Preparation of electrolyte (0.1M $NaHCO_3$) 1. Calculate and, accurately weigh Using a balance the Amount of Sodium Bicarbonate. 2. Dissolve the Sodium Bicarbonate in Deionized Water.	1. Sodium bicarbonate is a mild irritant and can cause irritation to the eyes and skin. 2. Can be spilled on the lab bench or floor, can create a slippery surface, leading to accidents.	1. Wear gloves and safety goggles. Wash hands thoroughly after handling. 2. Handle it under a fume hood. Clean up any spills immediately using paper towels.
Electrochemical testing for CO_2 reduction 1. Prepare the Electrochemical Cell. 2. CO_2 (1-30 bubbles per sec) saturation of the Electrolyte, the working pressure of CO_2 will be kept at atmospheric pressure (1 atm or 101.3 kPa). 3. Electrochemical Measurement Techniques – LSV, CA, CV (Voltage Range 0.5 V to -0.85 V).	1. Inappropriate design can waste 3D print materials and filaments, and more time elapsed on the experiment. 2. Lead to suffocation or dizziness if overexposed. 3. Lead to electrical shocks or short circuits if not handled properly.	1. Simulation should be done before 3D printing. 2. Use pressure regulators to control the CO_2 flow rate. Work in a well-ventilated area or fume hood. 3. Check all connections before and make sure all are grounded.
Have necessary measures been taken, that allows the activity to be performed in a safe manner ? Yes		Yes No – the work is not to be started